Journal of Power Sources 671 (2026) 239594

Contents lists available at ScienceDirect

Journal of Power Sources

journal homepage: www.elsevier.com/locate/jpowsour

Uncertainty in solid phase diffusivity determination: Comparing electrode parameterization workflows for P2D modeling of commercial battery cells

F. Röder [a,*], H. Harimi [a], F. Schomburg [a], M. Han [a], J.C. Wurzenberger [b], C. Lechner [b], S. Kutschi [b]

[a] University of Bayreuth, Bavarian Center for Battery Technology (BayBatt), Weiherstraße 26, Bayreuth, 95448, Germany
[b] AVL List GmbH, Hans-List Platz 1, Graz, 8020, Austria

GRAPHICAL ABSTRACT

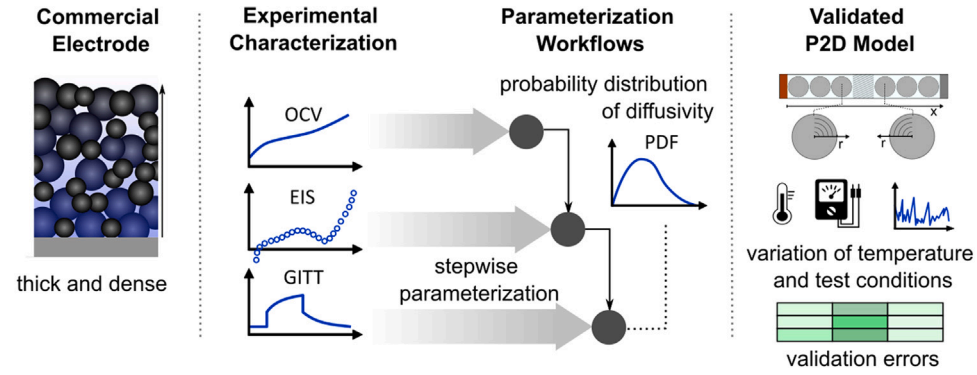

HIGHLIGHTS

- Investigation of the uncertainty of diffusion coefficient determination.
- Parameterization of commercial battery electrodes.
- Validation of P2D model parameterization workflows.
- Novel probability distribution function (PDF) based parameterization workflow.

ARTICLE INFO

Keywords:
Lithium-ion-batteries
Pseudo two dimensional battery model
Parameterization
Diffusivity
Validation

ABSTRACT

The pseudo-two-dimensional (P2D) battery model is a cornerstone of battery research, striking a critical balance between accuracy and computational efficiency for mathematical modeling of battery cells. It captures essential mechanistic parameters while remaining applicable for optimizing battery design and operation. It also often serves as the basis for aging modeling, a key challenge in the advancement of lithium-ion battery technology. However, wider adoption of P2D models is hindered by parameterization challenges, in particular the demanding time and experimental requirements of direct measurement strategies that preserve the full value of physically meaningful parameters. Among these, the solid phase diffusion coefficient, which is highly dependent on the lithium concentration in the active material particles, is particularly challenging. While Galvanostatic Intermittent Titration Technique (GITT) is widely used to measure it, its assumptions break down in phase-change materials and thick porous electrodes as used in commercial battery cells. This work evaluates

* Corresponding author.
E-mail address: fridolin.roeder@uni-bayreuth.de (F. Röder).

https://doi.org/10.1016/j.jpowsour.2026.239594
Received 26 September 2025; Received in revised form 5 February 2026; Accepted 7 February 2026
Available online 17 February 2026

different methods for determining diffusion coefficients, focusing on their impact on parameter plausibility and model accuracy under dynamic driving conditions. A novel approach is introduced to identify invalid GITT measurements and probability distribution of diffusion coefficient, allowing the construction of accurate models with plausible parameters.

1. Introduction

The development and understanding of modern technologies rely on the utilization of mechanistic models. They are essential for predicting system behavior, optimizing processes, and advancing innovations in various industries. In the realm of batteries, one of the most relevant mechanistic model is the pseudo-two-dimensional (P2D) model developed in the 1990s by Doyle, Fuller, and Newman [1]. This model serves as a cornerstone for model-based diagnostics, control, and optimization in battery research and development. Over the years, countless publications have built upon this model, reflecting its foundational role in the field. Moreover, the P2D model has been significantly extended to incorporate various phenomena, such as particle size distribution [2] and conductive networks [3], phase-change materials [4], aging mechanisms [5], thermal effects [6], and more. These extensions make it a versatile tool for capturing the multifaceted behavior of batteries under different conditions. However, the utility of this model family strongly depends on the availability of a valid parameter set [7]. The parameterization of the P2D model is challenging because it involves more than 30 parameters, many of which are not directly identifiable using full-cell voltage measurements in the time domain, and being often the bottleneck in wider adoption of the model [7,8]. As a result, sophisticated approaches are required to address these challenges. Such efforts are critical for advancing the use of mechanistic models in battery diagnostics and optimization, ultimately supporting the development of more efficient, durable, and sustainable energy storage systems.

In general, two strategies for model parameterization can be distinguished [8]. The first aims at a direct measurement of each parameter. This approach uses specific experimental techniques applied to subcomponents of a battery cell [9–12]. As the internal cell information is usually not disclosed by the manufacturers, this also includes cell disassembly and post-mortem analysis [8]. The strategy usually requires different measurement techniques, sample preparation or special experimental test cells. For instance, microstructure analysis based on nano and micro computer tomography on prepared electrode slices can be used to determine tortuosity in the electrode pores [13]. In order to analyze certain measurement results, some parameters must be known or determined in advance. For example, diffusion coefficients are often determined by Galvanostatic Intermittent Titration Technique (GITT) analysis, but require, for instance, that the particle size is known. Therefore, stepwise parameterization procedures are often adopted [8,9]. The second strategy approaches the problem from a system perspective and aims to estimate parameters based on input–output behavior by finding a set of parameters that fit the experimental data best [8,14]. This often requires some form of model reduction, as certain parameters are not uniquely identifiable [14]. Within this group of methods, a further distinction can be made between single-stage approaches, which fit all parameters simultaneously, and multi-stage approaches, which fit groups of parameters in stages, targeting regions where they are particularly sensitive [14–16]. Machine learning techniques can also be used to identify parameters [8]. It is important to note that a clear distinction between these strategies is not always possible. Direct measurement strategies often require final model tuning to fit the experimental data, while parameter estimation strategies usually use at least open circuit potential (OCP) measurements of both electrodes [8,14]. In both cases, parameter identifiability [17], sensitivity analysis [16], design of experiments [18] and model validation are critical considerations [7,14]. The main advantage of direct measurement strategies is that they preserve the full range of physical parameters, which is essential for design optimization and for embedding aging models that rely on cell internal states that are lost through model reductions applied in estimation-based methods [8,14]. However, the main drawback is the significantly higher experimental effort required, with the outcome being highly dependent on the workflow and the interdependence of parameters throughout the procedure.

The solid diffusion coefficient is particularly difficult to determine. It depends on the state of the battery, i.e., concentration and temperature [7,19]. For some materials it can vary by orders of magnitude [10]. Nevertheless, it is most commonly approximated as a constant value [17]. Various methods have been used to measure it. These include Electrochemical Impedance Spectroscopy (EIS), Potentiostatic Intermittent Titration Technique (PITT), Intermittent Current Interruption (ICI) and GITT, the latter being the most commonly used [8,20,21]. Another possible method is the Atlung Method for Intercalant Diffusion and Resistance (AMIDR), which promises to determine diffusivity with a higher accuracy than GITT [22]. Most methods rely on the evaluation of constant current (CC) pulse responses to determine the diffusion coefficient [23]. The most commonly used method is evaluation by linear regression in square root of time plots referred to as GITT analysis. This approach however, is related to various pitfalls as has been examined earlier. An overview is provided in the critical review of Kang et al. [24], which points out that determined values are often inconsistent and range in orders of magnitude. Nickel et al. [25] show that in particular at low temperatures where charge transfer resistance becomes more significant different evaluation strategies can vary in orders of magnitude. They propose a combination with EIS to calculate the time constants of the transfer reaction before GITT analysis. Further, non-ideal potential-driven transport, i.e. instead of concentration driven diffusion, can be taken into account by direct fitting of diffusion models as proposed by Horner et al. [23]. Further, care must be taken with phase-change materials such as lithium iron phosphate (LFP) or graphite [21,26]. In two-phase regions, certain assumptions of the GITT method [27] are violated. In particular, in regions where the OCP is constant, i.e., the gradient with respect to DOL is zero. This typically results in erroneously low, theoretically zero, diffusion coefficients, often several orders of magnitude smaller than outside these regions. Nevertheless, some studies have evaluated GITT data from such electrodes for P2D model parameterization [10,11]. Some studies disregard certain values, i.e. those of the two-phase regions [12,28] or discard the GITT data altogether in favor of fitting constant diffusion coefficients to C-rate tests [9]. Finally, GITT analysis usually requires ideal samples, i.e. thin electrodes and approximately uniform particle size, deviations to this can lead to significant inaccuracy of the determined diffusivity [19]. Particularly, for commercial batteries, electrodes are usually rather thick and dense, which can lead to significant uncertainty of the determined diffusivity.

Kang et al. [24] offer recommendations to improve GITT analysis. Many address sample and material preparation. Unfortunately, this cannot be adopted for commercial or preprepared electrodes, which are often considered in P2D model parameterization. Therefore, it should be noted that differentiation is necessary between idealized electrochemical experiments that aim to evaluate the diffusivity of a material and the practical task of parameterizing the P2D model for a commercial battery cell. Unfortunately, commercial battery electrodes often have thick and dense coatings and the active material powder and precise formulation cannot be extracted with reasonable experimental effort. Usually, only electrode sheets can be extracted and characterized to parameterize the model. For the parameterization of such thick and dense electrodes, significant methodological advancement are required as outlined by Günhter et al. [19], which is therefore the objective of this study.

In this paper, we compare different heuristic workflows that primarily employ a direct measurement strategy at the electrode level, as well as steps that utilize parameter estimation methods. Our goal is to enable reliable parameterization for P2D modeling of commercial electrodes, providing a physically meaningful parameter set at beginning-of-life (BOL) and minimizing validation errors across different temperatures. To this end, we investigate particularly the challenges outlined above being related to determining solid phase diffusivity.

Beyond this immediate objective, physically meaningful parameters at the BOL are essential for reliable model-based aging diagnostics, end-of-life (EOL) evaluation and assessment of second-use potential, where parameters are adjusted to account for changes due to cell degradation. Further, it enables optimization of electrode design and manufacturing processes as long as parameters truly reflect the cell internal processes and limitations. Improved parameterization workflows as being proposed in this work, thus supports both diagnostics and design applications of mechanistic battery models.

It is noted that the scope of this work is limited to the BOL parameterization. Further, no larger scale effects such as heat conduction and exchange with the environment is considered. This will be relevant if larger cell formats or connected cells are considered.

Specifically, we examine three workflows that mainly vary in the determination of the solid state diffusion coefficient. The three considered options are: (I) the fitting of constant diffusion coefficients to C-rate tests; (II) Classical GITT analysis; and (III) the assessment and evaluation of the probability distribution function (PDF) of the diffusion coefficient in consideration of electrolyte and electrode transport processes. The first two strategies are often applied in the literature and serve as a reference. In this work, the third strategy is proposed as an alternative. Here, the measurement uncertainty of diffusion polarization potential is determined using Gaussian Process Regression (GPR) and the sensitivity of diffusion polarization potential determined by the P2D model in consideration of all other model parameters. Both are then used together to determine the diffusion coefficient and its PDF. The different options are evaluated based on their impact on the plausibility of the parameter set. Furthermore, errors in validation experiments using various validation tests, i.e. dynamic driving cycles, cycling with C-rate variation, and pulse tests at different temperatures are analyzed.

2. Methods

2.1. Experimental

2.1.1. Materials

Experiments were conducted on lithium-ion battery electrodes harvested from 60 Ah pouch cells of the Hyundai IONIQ 5 electric vehicle using graphite and $LiNi_{0.8}Mn_{0.1}Co_{0.1}O_2$ (NMC811) as active materials.

2.1.2. Optical characterization

Extracted electrodes were optically characterized using digital microscopy. It was performed using a Keyence VHX-7000 digital microscope. Top-view images were captured to characterize particle size. Subsequently, the coating of the electrodes was removed from one side in selected areas in a glove box (GS GLOVEBOX Systemtechnik) filled with argon. These samples were used to measure coating thickness using depth of field images at the edges of removed coatings. Further details on the performed characterization are outline in the SI.

2.1.3. Measurement cells

Electrodes have been characterized electrochemically in PAT-cells from EL-CELL in different configurations. The first configuration is a half cell configuration using 1M LiPF6 in EC:DMC (1:1 w:w) as electrolyte and a 260 μm glasfiber separator (ECC1-00-0210-O/X from EL-CELL) with Li reference electrode and Li as counter electrode. For both electrodes, i.e. NMC811 and graphite electrodes, cells have been assembled and are used to measure OCPs at different temperatures. The second configuration is a three-electrode configuration using 1M LiPF6 in EC:DMC (1:1 w:w) as electrolyte and a 260 μm glasfiber separator (ECC1-00-0210-O/X from EL-CELL) with Li reference electrode using NMC811 as positive electrode and graphite as negative electrode. This configuration has been used to perform GITT, C-Rate tests, EIS and dynamic validation profiles. The third configuration is a blocking electrolyte configuration based on the work of Landesfeind et al. [29]. This configuration uses a symmetric cell setup with 50 mM etrabutylammonium perchlorate ($TBAClO_4$) in EC:DMC (1:1 w:w) as non intercalating electrolyte and a glasfiber separator (ECC1-00-0210-O/X from EL-CELL) with Li reference electrode. This configuration has been used to characterize both electrodes, i.e. NMC811 and graphite electrodes. Finally, a conductivity configuration has been used to measure electrical conductivity of the electrodes. Here, symmetrical cells have been assembled for NMC811 and graphite electrodes without separator, i.e. enabling direct electrical contact of both electrodes, using a pure solvent mixture with EC:DMC (1:1 w:w). This aims for a chemical and mechanical environment being close to the condition in the other configuration but theoretically without ionic conductivity. Cells have always been assembled in a argon filled glove box (GS GLOVEBOX Systemtechnik).

2.1.4. Mechanical characterization of the separator

The 260 μm glasfiber separator has been extracted from a the PAT-cell separator (ECC1-00-0210-O/X from EL-CELL) and characterized mechanically to estimate its compression within the PAT-Cell. The characterization has been performed using a universal testing machine (inspekt duo from Hegewal &Peschke) to measure stress–strain curve and evaluate the strain at 40 N being the approximate stress within the PAT-cell as reported by EL-CELL. Results are not further discussed in the main manuscript, but provided in the SI.

2.1.5. Electrochemical characterization

Electrodes are characterized electrochemically using PAT-Cells from EL-CELL company in the different configurations as provided above in frequency and time domains.

OCPs were measured in half-cell configuration inside a climate chamber (Binder KB) using a Basytec CTS LAB cycler. Electrode potential was evaluated for working electrode vs. reference electrode. Approximately 30 SOCs have been adjusted by CC charging and discharging with C/10 followed by 3 h rest, respectively. For some steps, e.g., for lithiation of the graphite electrode at high DOLs, applied charging current has been reduced to avoid lithium plating and reaching the voltage limit too early. The tests have been performed at three temperatures being 0 °C, 20 °C and 50 °C for two cells assembled from each electrode. The raw data is shown in the SI.

Further cells were electrochemically characterized for parameterization inside a climate chamber (Binder KB) using a Basytec CTS LAB cycler. The experiments were carried out in three-electrode configuration at 25 °C if not stated differently. The parameterization protocol consists of two parts. The first part adjusts different SOCs of the cell and performs pulse tests for GITT analysis. CC pulses are applied at different SOCs and in both directions, charging and discharging. Individual SOC points are always adjusted starting from a reference point, i.e. a fully discharged cell. This makes the protocol more time-consuming compared to measuring one SOC point after another, but effectively minimizes SOC drift caused by side reactions. First, the SOC is adjusted with C/5 in the charging direction, starting with the first SOC point, i.e. 10% SOC, followed by 3 h rest. Afterwards a C/10 CC charging pulse is applied for 300 s followed by 2 h rest. Next, the SOC is adjusted back to the previous SOC in the discharge direction, and a discharge pulse is applied using the same rates and rest times as for charging. Afterwards, the SOC is reset to the reference point, and the next pair of SOCs with charging and discharging pulses are applied. At some SOCs, i.e., at 40% and 60%, additional temperature variations are performed. Temperatures within the climate chamber are adjusted to 0 °C, 10 °C, 40 °C and 50 °C, respectively. After each temperature

change, a rest time of 5 h is applied and followed by charging and discharging pulses. After each charging and discharging pulse, 2 h rest time is applied. The second part performs a C-rate test. Here, various full CC charging and discharging steps are performed. For charging C/20 and C/2 are applied. For discharging C/20, C/2, 2C and 5C are applied. Before charging or discharging, 0% or 100% SOC is adjusted by applying CV step with a current limit of C/50 followed by a 30 min rest, respectively. The parameterization protocol has been performed for four cells. The raw data is shown in the SI.

EIS has been measured at cells in three-electrode configuration at three different temperatures, i.e. 0 °C, 20 °C and 50 °C, and different SOCs. Cells have been cycled inside a climate chamber (Binder KB) using a Basytec CTS LAB cycler. EIS has been measured with a Zahner ZENNIUM PRO potentiostat. EIS were measured from SOC 0% to SOC 100% in 10% steps for the positive and negative electrode. SOCs have been adjusted with C/10 CC charging starting at 0% SOC. Two cells were characterized for each SOC and temperature.

EIS has been measured for two cells in blocking electrolyte configuration for each electrode inside a climate chamber (Binder KB) at 25 °C using a Zahner ZENNIUM PRO potentiostat. EIS is measured to determine tortuosity as proposed by Landesfeind et al. [29]. The raw data is shown in the SI.

EIS has been measured for one cell in conductivity configuration for each electrode inside a climate chamber (Binder KB) at 25 °C using a Zahner ZENNIUM PRO potentiostat. The raw data is shown in the SI.

2.2. Mathematical model

A P2D model was used as the mathematical framework. The model employs partial differential equations to describe diffusion in spherical particles, diffusion in the electrolyte, and electrical conduction in the solid and ionic conduction in the electrolyte domains.

The equilibrium potential of the electrodes is provided as a function of concentration and temperature, using the Redlich–Kister equation [30] and a polynomial to describe entropy. Electrolyte diffusivity, transference number, and ionic conductivity are modeled using concentration and temperature dependent parameters [31]. It should be noted that parameterization of the electrolyte is very demanding and beyond the scope of this work, which focuses on the electrode parameterization. In our opinion, a less sophisticated parameterization of the electrolyte, i.e., reducing the effects of the electrolyte to concentration-dependent conductivity and constant diffusivity and transference number, is not an appropriate alternative. Therefore, we rely on the electrolyte parameters as provided by Landesfeind et al. [31] for the same electrolyte as used in this work. A sensitivity study for the parameterization with respect to variations of the electrolyte parameters has been performed and is provided in the SI. Reaction rates are calculated using a concentration-dependent Butler–Volmer equation, with temperature dependency incorporated through an Arrhenius term. The solid diffusion coefficient is modeled using the function

$$D_s(x_s, T) = D_{s,0}(x_s) \cdot \exp\left(\frac{E_{a,D_s}}{\mathrm{R}} \cdot \left(\frac{1}{T_{D_s,\mathrm{ref}}} - \frac{1}{T}\right)\right) \tag{1}$$

that depends on the DOL in the solid x_s and the temperature T. Temperature dependency is defined by the activation energy of diffusion E_{a,D_s} and the reference temperature of diffusion $T_{D_s,\mathrm{ref}}$. Further, the concentration dependent reference diffusion coefficient is given by

$$D_{s,0}(x_s) = \exp\left(S(x_s \cdot c_{\max})\right) \tag{2}$$

using the maximum concentration in the solid active material $c_{s,\max}$ and a Spline S that is given as

$$S(p_{c,i}) = \ln(p_{D_s,i}) \tag{3}$$

with concentrations $p_{c,i}$ and diffusion coefficients $p_{D_s,i}$ being the model parameters. As such the concentration dependency is an empirical function to be determined from measurement data. It is noted that we implement the electrochemical double layer according to Legrand et al. [32], which corresponds to minor differences with respect to classical implementations according to the Battery Parameter Exchange (BPX) Standard (bpxstandard.com). The deviations are discussed in more detail in the SI. All governing equations are provided in the SI.

We apply the assumptions that are commonly used for this model. The most relevant assumptions are:

- Fickian diffusion in the solid and electrolyte
- Uniform particle size
- Porous electrodes are modeled by means of effective transport parameters
- Buttler–Volmer reaction kinetics
- Electrode potentials are approximated by mean potentials, i.e. voltage hysteresis is not considered

These assumptions are naturally linked with deviations to experimental data. It should be noted that, in principle, phase-change materials require replacing the Fickian diffusion assumption by more appropriate models [4]. This applies to both, the model and the GITT analysis [26]. Nevertheless, fickian diffusion is most commonly used in P2D model frameworks, even for phase-change materials such as graphite. The goal of this work is not to improve the model, but to establish a workflow that improves the parameterization under the most common assumptions of this model.

The partial differential equations are discretized in space domain using finite volume method and the resulting set of ordinary differential equations is integrated in time domain using the ODE15s solver in MATLAB.

2.3. GITT analysis and its assumptions

In this and other works on P2D model parameterization, the polarization of pulses is evaluated to identify the diffusion coefficient. This process is referred to as GITT analysis. Therefore, most relevant assumptions of the GITT analysis are discussed in this section. According to [25], pulse measurements can be analyzed using

$$D_s^{\mathrm{GITT}} = \frac{4}{9 \cdot \pi} \cdot \left(\frac{R_{\mathrm{AM}}}{\Delta t} \cdot \frac{\Delta E_{\mathrm{OC}}}{\frac{\mathrm{d}E}{\mathrm{d}\sqrt{t}}}\right)^2 \tag{4}$$

to determine the diffusion coefficient, where R_{AM} is the particle radius of the active material, ΔE_{OC} is the change in open circuit voltage and $\frac{\mathrm{d}E}{\mathrm{d}\sqrt{t}}$ is the gradient of the potential versus the square root of time. Eq. (4) is frequently used and the diffusion coefficient can be determined using a linear fit of the potential against the square root of time:

$$\frac{\mathrm{d}E}{\mathrm{d}\sqrt{t}} = \frac{\Delta E}{\sqrt{\Delta t}} = \text{const.} \tag{5}$$

where ΔE is the diffusion polarization potential. According to [25], diffusion coefficients can be determined with 5% accuracy if

$$\tau_{\mathrm{pulse}} = \frac{R_{\mathrm{AM}}^2 \cdot t_{\mathrm{pulse}}}{D_s} < 0.0032 \tag{6}$$

with t_{pulse} being the pulse duration. Thus, Eq. (4) is valid for small diffusion coefficients or large particle sizes. However, the equation is derived from the analytical solution for constant current charging of a single particle as shown by Nickol et al. [25]. Therefore, one could also directly fit the analytical function, which will overcome the limitation.

However, further limitations persist. In this work, we investigate two issues that limit the practical applicability of GITT analysis for P2D model parameterization, in particular for commercial electrodes. The first limitation is related to phase-change materials and regions of the OCP that are flat and have non-smooth changes. The second limitation is related to the fact that the electrode is not an ideal single particle; the diffusion polarization potential is influenced not only by solid-state diffusion, but possibly also by the electrolyte and transfer reactions.

2.3.1. Nonlinear or constant electrode potentials

For the application of Eq. (4) it is assumed the gradient of the potential is constant and not zero. This assumption is not met for phase-change materials because they have regions with flat OCPs and significant gradient changes at the edges of the phase-change regions. Nevertheless, our goal is to automate the processing of pulse response data for such materials, which requires evaluating the violation of this assumption and, ideally, estimating the associated error, which is described below.

Using Eq. (5), the polarization potential can be calculated as

$$\Delta E = \sqrt{\Delta t} \cdot \frac{\mathrm{d}E}{\mathrm{d}\sqrt{t}} \tag{7}$$

Assuming the OCP gradient remains constant during the pulse, the diffusion polarization potential can also be expressed as:

$$\Delta E = \frac{\mathrm{d}E_{OC}}{\mathrm{d}x} \cdot \Delta x_1 \tag{8}$$

Here, Δx_1 represents the change in the DOL at the particle surface during the pulse. The change in open circuit voltage can be expressed accordingly as:

$$\Delta E_{\mathrm{OC}} = \frac{\mathrm{d}E_{OC}}{\mathrm{d}x} \cdot \Delta x_{\mathrm{OC}} \tag{9}$$

with Δx_{OC} being the average change in DOL, which can be calculated as

$$\Delta x_{\mathrm{OC}} = \frac{I_p \cdot \Delta t}{C_{\mathrm{abs}}^{\mathrm{Ah}}} \tag{10}$$

with I_p being the applied current during the pulse, which is defined positive in lithiation direction, and $C_{\mathrm{abs}}^{\mathrm{Ah}}$ being the total Ah capacity of the electrode. Rearranging this relationship allows to compute Δx_1 from the diffusion polarization potential:

$$\Delta x_1 = \frac{\Delta E}{\frac{\mathrm{d}E_{OC}}{\mathrm{d}x}} \tag{11}$$

Substituting Eq. (8) into Eq. (5) and then together with (9) into Eq. (4), provides an alternative expression for the diffusion coefficient:

$$D_s^{\mathrm{GITT},2} = \frac{4}{9 \cdot \pi} \cdot \left(\frac{R_{\mathrm{AM}} \cdot \Delta x_{\mathrm{OC}}}{\sqrt{\Delta t}} \cdot \frac{1}{\Delta x_1} \right)^2 \tag{12}$$

This shows that the identified diffusion coefficient is inversely proportional to the square of the change in the DOL at the surface:

$$D_s^{\mathrm{GITT},2} \propto \left(\frac{1}{\Delta x_1} \right)^2 \tag{13}$$

If the OCP gradient becomes zero, Δx_1 approaches infinity, causing the diffusion coefficient to drop to zero. This highlights why GITT analysis is invalid in phase-change regions where the OCP remains constant.

To estimate the error that is introduced by assuming a constant gradient, the change in lithiation polarization and its effect on the diffusion coefficient can be analyzed as:

$$D_s \propto \left(\frac{1}{\Delta x_1 + \epsilon_{\Delta x}} \right)^2 \tag{14}$$

Here, the error in the change of the DOL is defined as:

$$\epsilon_{\Delta x} = \Delta x_{\mathrm{true}} - \Delta x_1 \tag{15}$$

Although the true lithiation change Δx_{true} is unknown, it can be approximated using the measured diffusion polarization potential ΔE according to Eq. (7) and the nonlinear electrode potential $E(x) = f(x)$. This relationship is given by:

$$E(\hat{x} + \Delta x_2) = E(\hat{x}) + \Delta E \tag{16}$$

where $\hat{x}$ is the DOL before the pulse and ΔE is the diffusion polarization as calculated by Eq. (7). This accounts for any nonlinear changes in the potential over the lithiation change. Using the inverse of the potential function $x(E) = f^{-1}(E)$, the lithiation change can be calculated as:

$$\Delta x_2 = x(\hat{E} + \Delta E) - \hat{x} \tag{17}$$

with $\hat{E} = E(\hat{x})$. This alternative calculation provides a method to estimate the diffusion coefficient using Δx_2 instead of Δx_1. However, it is noted that Δx_2 is not the true lithiation change and is also not suitable for calculating the diffusion coefficient when the constant gradient assumption is violated. Nevertheless, under valid GITT conditions, Δx_2 and Δx_1 are approximately equal.

This allows for an estimate of the error in diffusion coefficient measurement due to nonlinearity violations:

$$\epsilon_{D_s^{\mathrm{GITT}}} = \frac{4}{9 \cdot \pi} \cdot \left(\frac{R_{\mathrm{AM}} \cdot \Delta x_{\mathrm{OC}}}{\sqrt{\Delta t}} \right)^2 \cdot \left[\left(\frac{1}{\Delta x_2} \right)^2 - \left(\frac{1}{\Delta x_1} \right)^2 \right] \tag{18}$$

The relative error can then be expressed as

$$\hat{\epsilon}_{D_s^{\mathrm{GITT}}} = \left| \frac{\epsilon_{D_s^{\mathrm{GITT}}}}{D_s^{\mathrm{GITT}}} \right| \tag{19}$$

This approach provides allows the evaluate the impact of nonlinearity in lithiation changes on the accuracy of GITT-derived diffusion coefficients.

2.3.2. Contribution of the electrolyte transfer reaction

For GITT analysis it is assumed that the electrode behaves like a single particle. However, real electrodes consist of an assembly of particles, and the charging conditions of the single particles vary significantly with position within the electrode. Furthermore, the electrolyte itself includes diffusion processes and, therefore, diffusion polarization potential. Finally, the reaction may influence the diffusion polarization potential. Thus, these assumptions are usually not met, particularly in thick-coated commercial electrodes. Additionally, electrodes usually do not have uniform particle sizes. However, since this is also a common assumption of the P2D model, this aspect will not be discussed here.

This work examines the influence of the electrolyte and transfer reaction on pulse polarization and, consequently, on the GITT analysis. Therefore, two modified versions of the P2D model are employed. The first modification cancels out the influence of the solid diffusion coefficient by replacing the solid diffusion equation (as shown in Table 1 in the SI) with

$$\frac{\mathrm{d}c_s}{\mathrm{d}t} = 0 \tag{20}$$

Thus, this model only considers reaction and electrolyte. The second modification further assumes that there is no reaction resistance, which corresponds to replacing equation for the intercalation current density, j_{Li} (as shown in Table 2 in the SI) by

$$j_{\mathrm{Li}} = j \tag{21}$$

with j being the absolute current density. Further the equations for the electrode potential, $\Delta\Phi$, (as shown in Table 1 in the SI) is replaced by

$$\Delta\Phi = E_{eq}(T, x_s, x_e) \tag{22}$$

with E_{eq} being the equilibrium potential. Since the solid concentration $x_s = c_s/c_{\mathrm{max}}$ does not change according to Eq. (20) and temperature, T, is constant, it is only influenced by the relative concentration in the electrolyte x_e. Thus, this modified model only considers the electrolyte contribution.

2.4. P2D model parameterization workflows

The mathematical model was parameterized using three different workflows. It is noted that these workflows are heuristic, drawing on experience and knowledge from literature, and other alternative

Table 1
Result of the parameter validation with Pulse Test, Cycling with C-Rate variation and WLTP Driving Cycles at different temperatures. Green level of the background indicates relative differences between the values, while red color indicates the lowest errors.

	workflow		
Error	$D_s = const$	*GITT-based*	*PDF-based*
Pulse test			
RMSE 10 °C / mV	19.84	21.13	18.63
RMSE 25 °C / mV	11.23	15.89	8.09
RMSE 40 °C / mV	11.04	9.49	7.61
C-Rate test (capacity)			
RMSE 10 °C / As	3.89	6.80	4.06
RMSE 25 °C / As	2.37	6.58	0.80
RMSE 40 °C / As	3.35	5.61	1.46
C-Rate test (energy)			
RMSE 10 °C / Ws	15.47	26.40	15.78
RMSE 25 °C / Ws	8.86	24.80	2.73
RMSE 40 °C / Ws	12.07	20.79	5.07
Driving cycle			
RMSE 10 °C / mV	24.28	44.26	29.95
RMSE 25 °C / mV	29.33	22.35	15.88
RMSE 40 °C / mV	26.84	15.55	19.19

heuristics are possible. All worfklows have in common that they primarily rely on direct measurements on electrode level, though parameter estimation is also included in some evaluation steps. Further, direct measurements are limited to those at the electrode level and include electrochemical measurements and digital microscopy, which are available in most labs.

Parameters are grouped and identified through four consecutive steps for all considered workflows. The parameter groups within each step are independent of each other, but dependent on preceding steps. Due to this interdependency, every change in a parameter can lead to deviations in consecutive steps. Thus, each step of the parameterization procedure contributes to the final result: the plausibility of the final parameter set and, most importantly, the predictive capability of the model.

Most evaluation steps are equal for the considered workflows. In the first step, OCV measurements in half-cell setups are conducted to measure OCPs and entropy changes at different degrees of lithiation, which are then approximated by a function. Additionally, basic assumptions and theoretical calculations are applied to set particle roughness and maximum concentration. Finally, geometric parameters, being electrode thickness and particle radius, are determined using digital microscopy. In the second step, information from the first step is used to adjust the active and passive material fractions to match the measured electrode capacities. Step three involves measuring the exchange current density, including its dependence on concentration and temperature. Exchange current density is identified by evaluating EIS using a R-RC equivalent circuit model. Further details on each evaluation step are provided in the SI.

Additional experiments are performed to determine tortuosity and electrical conductivity. Tortuosity is determined based on the work of Landesfeind et al. [29] by evaluating EIS in symmetrical cells filled with a blocking electrolyte using a simplified transmission line model (TLM-Q). Electrical conductivity is determined by evaluating the inner resistance of a symmetrical cell without a separator, i.e., when there is direct electrical contact. For both evaluation methods more details are provided within the SI.

The main focus of this work is the assessment of the diffusion coefficients, which is addressed differently, depending on the applied workflow. The three considered workflows are illustrated in Fig. 1. The figure shows the evaluation steps within the workflows, e.g., the evaluation of the OCP measurements. It also illustrates the number of parameters needed from previous evaluation steps by the thickness of the lines between the evaluation steps; thicker lines indicate more parameters. All workflows require four consecutive steps. Evaluation steps performed within one step are horizontally aligned. The main difference between the parameterization workflows is how the solid-state diffusion coefficient is determined. In brief, the three workflows are:

- Identification of the diffusion coefficient in step 4 using a C-rate test, assuming that it is independent on concentration and temperature, referred to as $D_s = const$ and illustrated in Fig. 1a.
- Identification of the diffusion coefficient in step 3 using GITT analysis, assuming that GITT analysis is independent on other processes such as electrolyte diffusion, referred to as *GITT-based* and illustrated in Fig. 1b.
- Identification of the diffusion coefficient and its PDF in step 4 by analysis of the pulse responses in consideration of all other parameters, which requires to determine tortuosity and conductivity in previous step, referred to as *PDF-based* and illustrated in Fig. 1c.

The evaluation step used to identify the diffusion coefficient is indicated with a colored arrow. The parameters used for this evaluation step are also indicated by colored flows. The influence on further evaluation steps is also indicated by colored flows.

The $D_s = const$ workflow uses a C-Rate test to fit all remaining parameters, being tortuosity (given by the Bruggeman coefficient), electrical conductivity and a constant and temperature independent diffusion coefficient.

The $GITT - based$ workflow identifies the diffusion coefficient and its temperature and concentration dependency using GITT analysis in step 3. However in step 3 tortuosity, electrical conductivity and the reaction kinetic is not yet identified. Thus, it is assumed that the influence of these processes on pulse polarization is negligible. After step 3, the remaining parameters, being tortuosity and electrical conductivity are identified using the C-rate test, similar to the $D_s = const$ workflow, but now in consideration of the diffusion coefficient.

For the *PDF-based* workflow, all parameters except the diffusion coefficient were identified in steps 1–3. This enables estimation of the diffusion coefficient while considering all other parameters and processes. First, the uncertainty of pulse polarization is evaluated using GPR. Second, the influence of the diffusion coefficient on pulse polarization is evaluated using the full-order P2D model. Note that tortuosity and electrical conductivity must be measured in dedicated experiments before evaluating the diffusion coefficient, which was not needed for the other workflows. Finally, the two are combined to identify the PDF of the diffusion coefficient. This assessment of the PDF is elaborated on in more detail in the following Section 2.5.

It should be noted that the applied workflows can also differ in terms of computational cost. The *PDF-based* workflow involves an additional step that requires significant computational effort: determining the influence of the diffusion coefficient on pulse polarization. This requires multiple executions of the full-order P2D model for constant current pulses. Conversely, the *PDF-based* workflow does not require parameter fitting using C-rate data, which also necessitates numerous P2D model executions. In general, the computational effort for data evaluation is not usually time-critical. Rather, the duration of the experiments determines how quickly one can identify the parameters. However, reducing experimental time, e.g. by reducing the number of

Table 2
Results for the parameters are shown for each workflow for tortuosity and electrical conductivity of the negative electrode (NE) and positive electrode (PE).

Parameter	Tortuosity \ -		Conductivity \ S m^{-1}	
Electrode	PE	NE	PE	NE
$D_s = const$	1.17	16.63	17.25	0.1
GITT-based	1	5.53	84.19	0.11
PDF-based	8.45	7.32	0.25	0.58

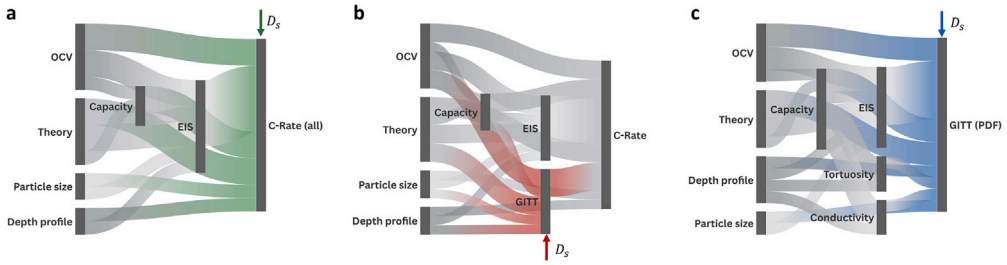

Fig. 1. Illustration of heuristic workflows, being (a) $D_s = const$, (b) *GITT-based* and (c) *PDF-based*, for stepwise P2D model parameterization. Each dark gray bar corresponds to an evaluation step. Evaluation steps performed within one step are aligned horizontally. The evaluation step used to estimate the solid-state diffusion coefficient (D_s) is indicated by a colored arrow. The flows between evaluation steps indicate parameters that serve as inputs or outputs. The width of the flows corresponds to the number of parameters. Input and output flows corresponding to the evaluation step for the diffusion coefficient are marked with colors.

pulse or EIS measurements, usually leads to less reliable parameters. Therefore, the goal of this work is not to reduce the time required for parameter estimation, but rather to focus on the reliability of the determined parameter set.

We aim to validate the workflows by two aspects. First, we evaluate the values that are determined differently, being tortuosity, electrical conductivity and the diffusion coefficient and discuss whether they are plausible. Further, we evaluate the deviations of the parameterized model in various validation tests, i.e. dynamic driving cycles, cycling with C-Rate variation, and pulse tests at different temperatures that have not been used for parameterization.

Identified parameter sets are provided in the SI.

2.5. Assessment of the PDF of the diffusion coefficient

The *PDF-based* strategy proposed in this work aims to overcome the limitations of the *GITT-based* assessment of the diffusion coefficient. The approach considers the measurement uncertainty and parameter sensitivity and combines both to calculate the PDF of the solid diffusion coefficient. To access the parameter sensitivity, the full-order P2D model is used, which also considers the electrolyte and reaction contribution to diffusion pulse polarization as determined in previous steps. It should be noted that the determined PDF of the diffusion coefficient depends on the electrolyte and reaction parameters, and will differ if different parameters are used. Finally, the concentration dependency of the diffusion coefficient is determined using the expected value of the PDF.

In the pulse measurement, a constant current pulse of 300 s is applied at different SOCs and temperatures. Diffusion processes, i.e. solid-state diffusion and diffusion within the liquid electrolyte, and possibly also the transfer reaction contribute to longer timescales, e.g. > 1 s, while electrical conductivity and reaction polarization mainly contributes to shorter timescales. Although there is no clear boundary between these processes, the response over a longer timescale is usually sensitive to solid diffusion.

The measurement uncertainty of the absolute polarization between $E_1 = E(t_{\text{pulse}} = 1\text{ s})$ and $E_2 = E(t_{\text{pulse}} = 300\text{ s})$, i.e. $|\Delta E| = |E_2 - E_1|$, is evaluated using GPR with measured values at different degrees of lithiation x_s. GPR is applied to model the conditional probability $p_{|\Delta E|}(|\Delta E| \mid x_s)$ as

$$p_{|\Delta E|}(|\Delta E| \mid x_s) = \mathcal{N}\left(|\Delta E| \mid \mu(x_s), \sigma^2(x_s)\right) \tag{23}$$

based on observed data points $(x_{s,i}, |\Delta E_i|)$. The model is trained in MATLAB using the `fitrgp` function with a rational quadratic kernel.

Further, we calculate $|\Delta E|$ using the P2D model with parameters as determined in steps 1–3 for grid of diffusion coefficients (ranging from 10^{-17} to 10^{-10} m^2s^{-1}) and DOL (ranging from 0.05 to 0.95). This used to determine

$$|\Delta E| = f(D_s, x_s) \tag{24}$$

using a 2D lookup table, in which values of $|\Delta E|$ are precomputed and stored for discrete combinations of (D_s, x_s). During evaluation, $f(D_s, x_s)$ is retrieved by interpolation.

Finally, both functions are combined to determine the PDF of the solid diffusion coefficient as

$$p_{D_s}(D_s \mid x_s) = p_{|\Delta E|}\left(f(D_s, x_s) \cdot \left|\frac{df(D_s, x_s)}{dD_s}\right| \mid x_s\right) \tag{25}$$

The equation is then evaluated to determine diffusion coefficient with the highest probability, $\max(p_{D_s})$, which is then used to fit the concentration dependent diffusion coefficient, i.e. Eq. (2).

3. Results and discussion

3.1. Assessment of the uncertainty in pulse polarization measurements

Experimental results for the pulse measurements are shown in Fig. 2. As an example, in Fig. 2a and b the time series data is shown for the pulse response at 50% SOC and 25 °C for the negative and positive electrode, respectively. The potential is shown as a change with respect to the potential before the pulse, E_0. In this example, the pulse is applied in charge direction, which leads to decline of electrode potential of the negative electrode, and an increase of the electrode potential of the positive electrode. The results show typical diffusive behavior with a declining gradient of the potential. Further, the electrode potential at 1 s, E_1, and 300 s, E_2, are indicated as x marker in red and blue, respectively.

The difference between E_1 and E_2, i.e. the diffusion polarization potential, ΔE, is shown in Fig. 2c and d as a function of DOL for the negative electrode and the positive electrode, respectively. The markers show all data points extracted from the pulses in lithiation (right pointed triangle) and delithiation (left pointed triangle). It can be seen that for the negative electrode, shown in Fig. 2c, ΔE is rather low, approximately 0.01 V for most of the data points. Only at very low degree of lithiations and at a DOL of approximately 0.5 the diffusion polarization potentials are higher. It is noted that these regions also correspond to larger OCP gradients. The diffusion polarization potential of the positive electrode, as shown in Fig. 2b, is in a similar range, but show more distinct differences at different DOLs. The highest values are observed at high and low SOCs and the lowest values at approximately 0.6.

The diffusion polarization potential data is analyzed further using GPR according to Eq. (23). This allows us to evaluate the uncertainty of the measurement. As can be seen by the 2σ range, the uncertainties are lower at DOLs where the measurement values are available. For the negative electrode, the highest values at very low SOCs have been excluded from the GPR. The very high values are related to the fact that the OCP is very steep here. Including these values leads to anomalies in the subsequent evaluation. At the end of the DOL spectrum, the uncertainty is highest because no more measurement values are available.

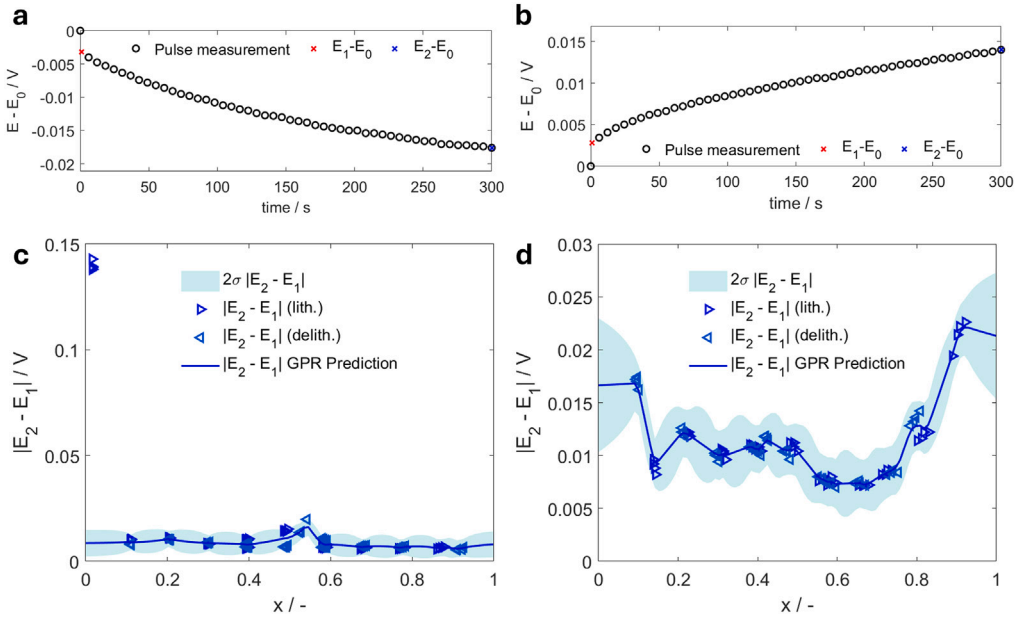

Fig. 2. Change of electrode potential for a CC charge pulse at 50% SOC and 25 °C of ((a) the negative electrode and b) the positive electrode. Black circles show the experimental data and red and blue x indicate the potential $E_1 - E_0$ at 1 s and $E_2 - E_0$ at 300 s, respectively. The absolute of the difference between the potential E_2 at 300 s and E_1 at 1 s at for all pulses as a function of DOL are shown for the (c) negative electrode and (d) the positive electrode. Markers indicate the value in lithiation (right pointed triangle) and delithiation (left pointed triangle). Solid lines show the prediction of the GPR model and the area indicates the $2 \cdot \sigma$ range.

In summary, the results of the pulse measurements show the typical polarization behavior due to diffusion processes, e.g., a declining polarization gradient and higher values at very high and low DOLs. Applying GPR further elucidates the uncertainty of the measured diffusion polarization potentials, which will be exploited to determine the PDF of diffusion coefficient.

3.2. Limitations of GITT analysis

As previously discussed, it is well known that GITT assumptions are not satisfied for measurements at porous electrodes and in particular when the active material exhibits flat regions of the OCP and the electrolyte contribution is significant. This section examines the limitations of GITT analysis in detail to better understand the applicability of the GITT method for P2D model parameterization. First, we discuss the consequences of assuming a constant, non-zero potential gradient. In this context, the negative electrode with very flat plateaus is investigated in particular. Second, a simulation study based on the P2D model is used to evaluate the influence of electrolyte.

In Eq. (4) we compare the results of the GITT analysis for two pulses that are located in different regions of OCP. The first pulse (Pulse A) is located at a DOL of approximately 0.7. at a rather flat region of the OCP. The second pulse (Pulse B) is located at a steeper region of the OCP at a DOL of approximately 0.1. For Pulse B a diffusion coefficient of approximately $1 \cdot 10^{-15}$ m^2 s^{-1} is determined while for Pulse B the diffusion coefficient is approximately $1 \cdot 10^{-18}$ m^2 s^{-1} and thus orders of magnitude lower.

This difference is related to the violation of GITT assumption regarding constant and non zero gradients. This can also be seen by evaluating the relative error according to Eq. (19), which is 0.036 for Pulse B and larger than 1e3 for Pulse A. The origin of the high relative errors in the GITT measurements is elaborated on in more detail below.

It is well known that the assumptions underlying GITT analysis are not valid for two-phase materials [21]. This is primarily due to the fact that, in these regions, the OCP is very flat, i.e., the gradient is approximately zero. However, GITT analysis relies on relating the change in OCP to the polarization potential to determine diffusivity.

In Figs. 3, the analysis of two GITT pulses (A and B) is shown. Fig. 3a depicts a pulse located within a two-phase region (Pulse A), while Fig. 3b shows results for a pulse located outside a two-phase region (Pulse B) as can depicted in Fig. 3c. The electrode potential during the pulses is plotted in Fig. 3a and b against the square root of time.

For Pulse A, it can be observed that the measured points follow an almost linear trajectory, as expected for Fickian diffusion. While one might argue that Fickian diffusion is not valid for two-phase materials, the results suggest that the process may still be reasonably well-described by this assumption. Thus, the measurement is then fitted with a linear function using the points within the darker yellow background. This region is automatically identified by evaluating linearity through the second derivative of the potential. By extrapolating to the beginning and end of the pulse, a polarization potential of −6.48 mV is obtained.

Similarly, in Fig. 3b, the same analysis is applied to Pulse B, which is located outside the two-phase regions. Here, a linear slope is also observed and is used to fit a linear function. This analysis results in a polarization potential of −11.89 mV, which is approximately twice as high as that for Pulse A.

Using Fig. 3c, the measured polarization potentials are analyzed in the context of the OCP. The curve in the figure represents the OCP during lithiation. The positions of Pulses A and B are labeled as 'x Pulse A' and 'x Pulse B', respectively. Additionally, the polarization potentials for Pulse A and Pulse B are represented by blue and yellow areas, corresponding to Figs. 3a and b. Under the assumption of Fickian diffusion in a single particle and no electrolyte contribution, this visualization allows the polarization potential to be translated into a corresponding change of DOL, Δx_2, which represents the DOL corresponding to the polarization potential. It can be observed that, although the polarization for Pulse A is smaller than that for Pulse B, the change of DOL (Δx_2) for Pulse A is significantly higher.

The GITT analysis assumes that the gradient of the OCP remains constant during the pulse, as the pulse only slightly deflects the system from its current DOL. Based on this assumption, a change of DOL, Δx_1, can be calculated as defined by Eq. (11) and be used to represent the diffusion coefficient expressed in Eq. (12) in the method section. However, if the gradient of the OCP is approximately zero, this calculation

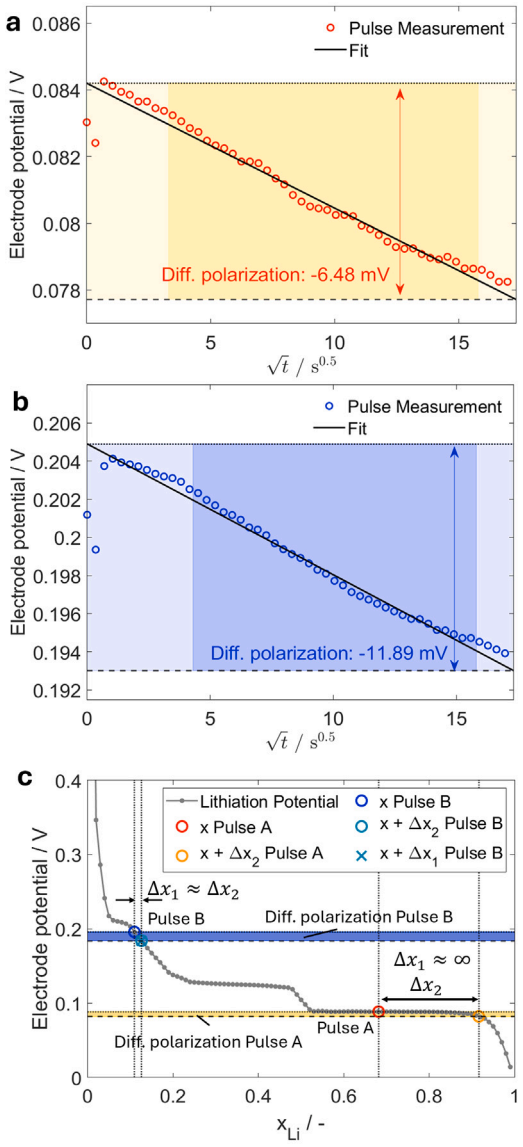

Fig. 3. (a) GITT-measurement and fit for example Pulse A in phase-change region, (b) GITT-measurement and fit for example Pulse B outside of phase-change region and (c) Illustration of pulse polarization in OCP vs. DOL graph.

leads to $\Delta x_1 \approx \infty$. Consequently, a significant discrepancy between Δx_1 and Δx_2 is observed.

In contrast, if the gradient of the OCP is not zero and is nearly constant within the polarization range of the pulse, as assumed by GITT, then approximately, Δx_1 will equal Δx_2. This relationship is used to derive the relative error, denoted as hat $\hat{\varepsilon}_{D_s}$, as described in the methods section. Note that this error estimate solely results from the OCP gradient not being constant; electrolyte influence has not yet been considered.

As can be seen, it is challenging to assess the diffusion coefficient in two-phase regions. The GITT method predicts an infinite change in DOL, resulting in a very low diffusion coefficient under these conditions. This results in very low diffusion coefficients in GITT analyses, which is commonly observed for graphite. Evaluating the relative error introduced in this work can detect the violation of this linearity and non-zero assumption.

Furthermore, the application of GITT analysis requires that the electrode behave like a single particle. However, for thick electrodes, the electrolyte can influence the pulse response, which violates this assumption. This will be examined in the following.

Applying Eq. (3) requires that the pulse time constant, τ_{pulse}, be less than 0.0032 to achieve a deviation of less than 5%, under the assumption of single-particle behavior. Thus, we investigate two cases: one where it is above this threshold and one where it is below. Fig. 4a and 4b show simulation results for a constant current pulse with $\tau_{\text{pulse}} = 0.001$ and $\tau_{\text{pulse}} = 0.01$, respectively. The colored solid lines correspond to simulations using the P2D model with different OCP gradients. The solid black line shows the result for the electrolyte alone, i.e., solid diffusion and transfer reactions are canceled out, as described in Section 2.3.2. The black dashed line shows the simulation results for the electrolyte and reaction; solid diffusion is canceled out, as described in Section 2.3.2. As can be seen, even without solid diffusion, a thick electrode exhibits diffusive pulse behavior due to diffusion processes in the electrolyte. In the presented simulation example, adding the reaction mainly leads to a parallel shift of the electrode potential. It is noted, that the reaction may also affect the diffusive part if the time constants are larger. By varying the gradient of the OCP, it can be seen that the impact of the solid diffusion coefficient depends strongly on the gradient of the OCP and is more distinct for steeper gradients. This effect is also visible in Fig. 2 for the measured pulse responses. The figure shows a larger diffusion polarization potential in regions where the OCP is steeper, i.e., at high and low SOCs, as well as at approximately 0.5 for the negative electrode. In theory, the influence of solid diffusion disappears for zero gradients.

The pulse responses are evaluated using a square root of time fit (sqrt time fit) with Eq. (4) and a direct fit of the analytical solution (analyt. fit). The results are shown in Fig. 3c for different OCP gradients. The solid black line indicates the diffusion coefficient normalized using the diffusion coefficient set in the model, $D_{s,\text{set}}$. The results for a diffusion time of 0.001 s are shown in blue. Circle markers indicate the analytical fit, and square markers indicate the square root of time fit. A significant deviation between the set value and the identified diffusion coefficients can be observed for both. In general, the diffusion coefficient is underestimated. The lowest deviations are observed with the steepest gradient of −0.5 V, where the deviation is approximately 20% for both fits. The analytical fit is only slightly better. The results for diffusion times of 0.01 s are shown in red. Deviations significantly increase for both methods, being lowest at the steepest gradients: approximately 30% for the analytical fit and approximately 40% for the square root of time fit. Under these conditions, the analytical fit generally leads to slightly lower deviations. Nevertheless, both approaches lead to significant deviations between the identified and set values for thick porous electrodes where the electrolyte contributes. Errors generally increase with decreasing potential gradients.

In summary, the GITT analysis can only be used to make a rough estimate of the diffusion coefficient if the OCP gradient is large, non-zero, and constant, and if τ_{pulse} is small. Errors resulting from a violation of the constant gradient condition can be estimated using the proposed value of the $\hat{\varepsilon}_{D_s}$. This will be particularly important for materials that exhibit flat OCPs. Further, the electrolyte contribution must also be considered. This is particularly important if the diffusion coefficient is high and the OCP gradient is low. Generally, using the P2D model directly to evaluate the pulse could overcome most of the limitations of GITT analysis in thick electrodes, as this model considers the electrolyte contribution and non-constant OCP gradients. However, in phase-change regions, where the gradient of the OCP is zero, pulse responses cannot be reliable evaluated and should be excluded.

3.3. Uncertainty of the diffusion coefficient

Section 3.1 showed that measuring diffusion polarization potentials is associated with uncertainties. Furthermore, Section 3.2 showed that analyzing diffusion polarization potentials with GITT can lead to significant errors if the assumptions are not met. Therefore, this section

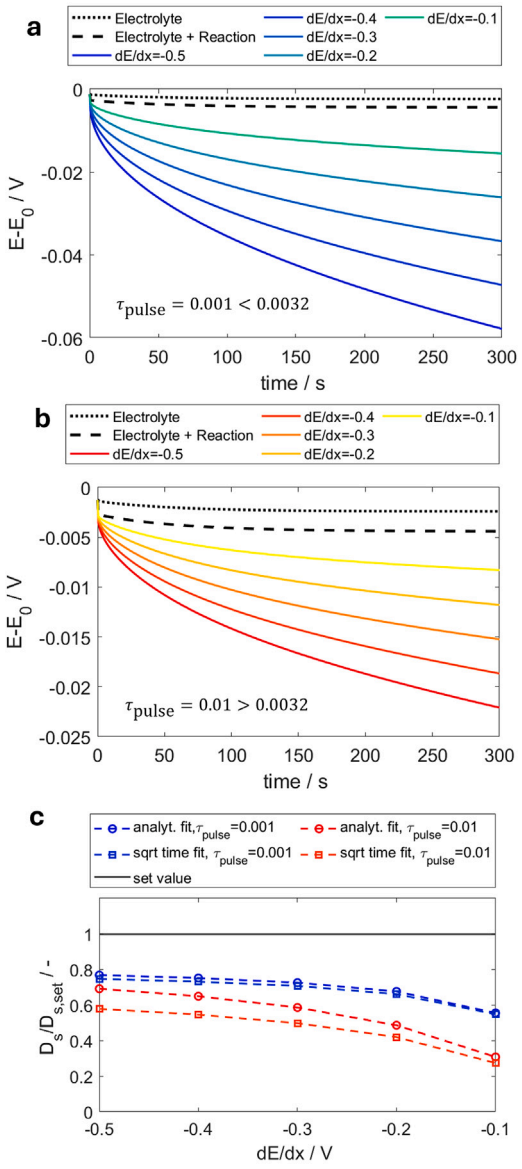

Fig. 4. Simulation results for pulse polarization for various constant OCP gradients, dE/dx, given as solid lines and model variants with only electrolyte (dotted) and only electrolyte and reaction (dashed) contribution for diffusion coefficients that lead to (a) $\tau_{pulse} = 0.001$ and (b) $\tau_{pulse} = 0.01$. (c) Results for GITT analysis with linear square root of time fit (red) and fit of the analytical equation (blue) as diffusion coefficient normalized by the set value, which is indicated as black solid line. (For interpretation of the references to color in this figure legend, the reader is referred to the web version of this article.)

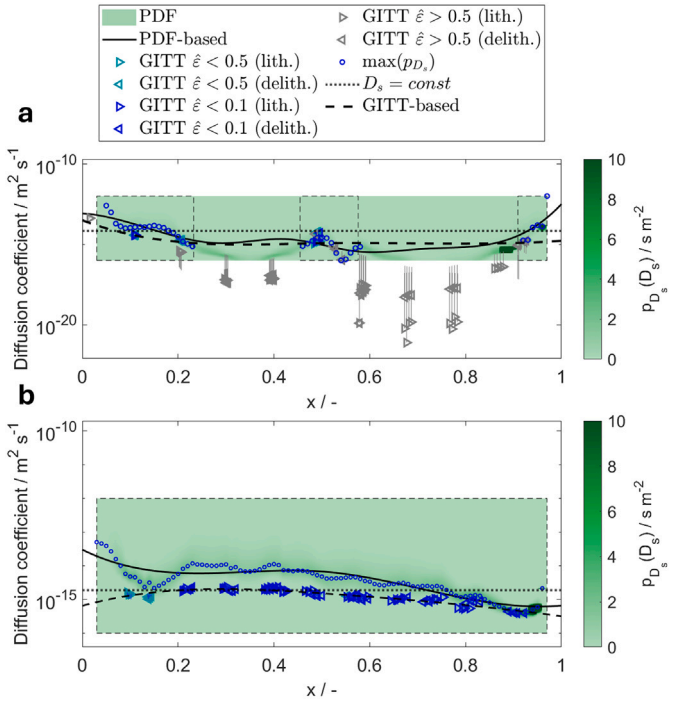

Fig. 5. The diffusion coefficient is shown as a function of DOL (x) for the (a) negative and (b) positive electrodes. The PDF of the diffusion coefficient is shown in green as a colormap, and the maximum probability is indicated by blue circle markers for selected DOLs. The results of the GITT analysis are shown as markers: right-pointing triangles for lithiation and left-pointing triangles for delithiation. The color of the markers indicates the relative errors, and the vertical bars indicate the absolute errors. The areas included for parameter identification with GITT- and *PDF-based* approaches are indicated by dashed rectangles. The results for $D_s = const$ (dotted), *GITT-based* (dashed) and *PDF-based* (solid) are shown. (For interpretation of the references to color in this figure legend, the reader is referred to the web version of this article.)

investigates the probability density function (PDF) of the diffusion coefficient, as introduced in Section 2.5.

To evaluate the diffusion coefficient, the tortuosity and electrical conductivity were determined using EIS data from symmetrical cell configurations. Tortuosity was determined to be 7.32 and 8.45 for the graphite and NMC811 electrodes, respectively. Electrical conductivity was determined to be 0.58 and 0.25 for the graphite and NMC811 electrodes, respectively. More details on the evaluation and results are provided in the SI. Note that the results for the *PDF-based* method depend on these values.

Figs. 5a and 5b show the diffusion coefficients for the negative and positive electrodes, respectively. The triangle markers indicate the diffusion coefficients as determined by GITT analysis using the square root of time fit. The type of marker indicates the direction of lithiation (right-pointing triangle) or delithiation (left-pointing triangle). Furthermore, the relative error, $\hat{\varepsilon}_{D_s}$, is indicated by the color code, where darker blue indicates the lowest errors (i.e., < 0.1), lighter blue indicates errors < 0.5, and gray indicates values with high errors (i.e., > 0.5). The estimated absolute error, $\hat{\varepsilon}_{D_s}$, is indicated by a vertical line for each GITT data point. The shaded areas show the result of the PDF as determined by Eq. (25). Blue circles indicate the diffusion coefficient at the maximum of the PDF for various DOLs. Dashed rectangles indicate the area used to identify the diffusion coefficient in the *PDF-based* and *GITT-based* approaches. Regions with flat OCPs are excluded. We excluded regions where the absolute delithiation OCP gradient was smaller than 0.2.

The results for the negative electrode is shown in Fig. 5a. It can be seen that the diffusion coefficients determined by the GITT analysis deviate in orders of magnitude, with lowest values of smaller than 10^{-20} m^2 s^{-1} to 10^{-12} m^2 s^{-1}. Lowest values are observed between a DOL of 0.25–0.45 and 0.55–0.85, corresponding to a flat OCP as can be seen in Fig. 5c. In this region also very high relative errors $\hat{\varepsilon}_{D_s} > 0.5$ are observed, which indicates that the condition of a constant and non zero OCP gradient are not fulfilled. Values that fulfill the condition are found at DOLs between 0.1–0.2 and at approximately 0.5. Evaluating the PDF of the diffusion coefficients indicates in general higher diffusion coefficients. Within the two-phase region the observed slope follows the trend that can be determined by GITT and the absolute error of the GITT. It is lowest at the center of the two-phase regions, i.e. at a DOL

of approx. 0.35 and 0.75. Towards the edges of the two-phase region it increases. This observation can be explained as follows. To obtain a diffusion polarization response in a two-phase region, the diffusion coefficient must be low enough to cause a change in DOL, Δx, that extends beyond the two-phase region. The required diffusion coefficient is lowest at the center of the two-phase region. As this is essentially the same process used to assess the change in DOL, Δx_2, this also explains why both follow the same trend. However, this is only an anomaly of this analysis, so the values in the two-phase regions are disregarded in any further analysis, i.e. *GITT-based* and *PDF-based* workflows.

The results of the positive electrode is shown in Fig. 5b. Results of the GITT analysis show highest values at medium DOLs and lower values at high and low DOLs. All values have low relative errors, $\hat{\varepsilon}_{D_s} < 0.5$. The PDF of the diffusion coefficients is also rather flat, showing only low probabilities, whereas the highest probabilities are found at higher values compared to the GITT analysis. The most significant deviations are found at DOLs, where both methods indicate higher diffusion coefficients. This observation is consistent with our previous analysis, which showed that GITT tends to underestimate diffusion coefficients, with larger deviations for larger τ_{pulse}, i.e. larger diffusion coefficients.

The results for the positive and negative electrodes are then used to identify the diffusion coefficient as a function of concentration, i.e., the DOL. Two different approaches are used to accomplish this. The first approach uses GITT data points and is GITT-based. It is indicated by a dashed line in Fig. 5. The second approach uses the maximum values of the PDF of the diffusion coefficient and is indicated by a solid line in Fig. 5. For the negative electrode (Fig. 5a), it can be seen that the diffusion coefficient is generally higher with the *PDF-based* approach, except for the second plateau of the graphite OCP. Furthermore, it can be seen that an increase in the diffusion coefficient can be observed at high DOLs with the *PDF-based* approach. This is not visible for the *GITT-based* analysis. For the positive electrode (Fig. 5b), the diffusion coefficient shows a similar slope to the *GITT-based* method but with higher values. Only at very low DOLs is the slope different; it increases, in contrast to the *GITT-based* method, where it decreases.

The PDF was evaluated for temperature variations at 40% and 60% SOC. The results are shown in Fig. 6. The figure shows the logarithm of the diffusion coefficient as a function of T^{-1}, i.e., an Arrhenius plot. Figs. 6a and 6c show the results for the negative electrode. As can be seen, the probabilities are generally rather low, i.e., the distribution is wide. A linear fit was identified in the Arrhenius plot using the maximum probability. The gradient of the linear function is then used to calculate the activation energy. Optimization yields an activation energy of 4.2 kJ. At 60% SOC, a gradient can be observed, yielding an activation energy of 11.9 kJ mol^{-1}.

The PDF of the positive electrode is shown in Figs. 6b and 6d. The activation energies are 9 kJ mol^{-1} and 11.3 kJ mol^{-1} for 40% and 60% SOC, respectively. Higher probabilities are observed at low temperatures, as can be seen. This is because the diffusion coefficient is lower in this region, indicating greater sensitivity to the diffusion polarization potential.

In summary, evaluating the PDF of the diffusion coefficient enables evaluation of diffusivity considering measurement uncertainty and sensitivity. In general, the PDF indicates higher values than the GITT analysis. The highest differences are observed in regions with flat OCPs (i.e., the negative electrode) and for high diffusion coefficients (i.e., medium DOLs of the positive electrode).

3.4. Validation of the model parameters

This section investigates the impact of the three possible workflows for parameterizing the P2D model: $D_s = const$, *GITT-based*, and *PDF-based*.

Figs. 7a-f show the simulation and experimental results of the C-rate test for the negative and positive electrode potentials in the *PDF-based*, *GITT-based*, and $D_s = const$ workflows. Note that the C-rate test was used to estimate the final set of parameters for the $D_s = const$ and *GITT-based* workflows. In contrast, the *PDF-based* workflow does not include the C-rate test data in the model parameterization. In this case, however, it can be used to validate the workflow.

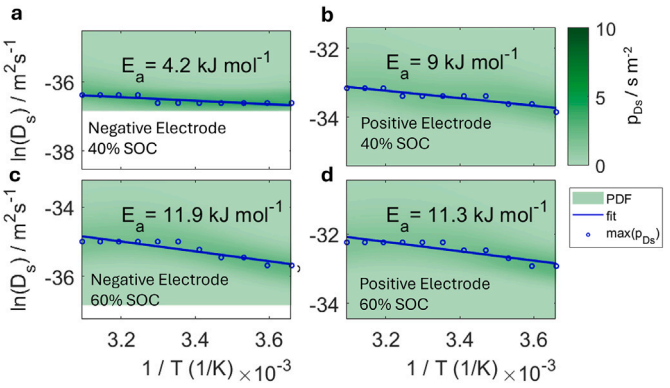

Fig. 6. The logarithm of the diffusion coefficient is plotted against $1/T$ for (a) the negative electrode at 40% SOC, (b) the positive electrode at 40% SOC, (c) the negative electrode at 60% SOC and (d) the positive electrode at 60% SOC. The PDF of the diffusion coefficient is indicated as colormap in green. The maximum of the diffusion coefficient is indicated as blue circle. The linear fit to the maximum values is shown as blue solid line and the corresponding activation energy of diffusion is given. (For interpretation of the references to color in this figure legend, the reader is referred to the web version of this article.)

Figs. 7a and 7b show the results for the $D_s = const$ workflow for the negative and positive electrodes, respectively. There is a very good agreement between the simulation and experimental data. For the negative electrode, small deviations are visible at the beginning of charge at C/2 and at the end of discharge at 1C. For the positive electrode, deviations are visible during 2C discharge. The overpotentials are overestimated here, which is most evident in the center of the discharge curve. Small deviations are also visible at the end of discharge with 5C. Charging with C/2 shows that the overpotentials are higher, and the potential is overestimated between 10 and 25 As.

More significant discrepancies are observed for the *GITT-based* workflow. Fig. 7c shows the results for the *GITT-based* workflow for the negative electrode potential, where some deviations are evident. In particular, significant deviations are visible towards the end of discharge for discharging with C/2 and 2C. Surprisingly, there is very good agreement for the highest and lowest discharge rates, i.e., 5C and C/20, respectively. Additionally, when charging with C/2, the voltage drops at approximately 22 As. The voltage then reaches 0 V, often considered the offset potential for Li-plating. Consequently, the model predicts Li-plating to occur earlier than the $D_s = const$ workflow. The results for the positive electrode are very similar to those of the $D_s = const$ workflow. Deviations are mostly visible during 2C discharge and C/2 charge; overpotentials are overestimated in both cases. Slightly higher deviations are visible at the end of the C/2 discharge.

Fig. 7e shows the results for the *PDF-based* workflow for the negative electrode. A good agreement with the experimental data can also be observed. No significant deviations are visible for charging and discharging below C/2. However, when discharging at higher rates, the potentials are underestimated towards the end of the discharge process. Nevertheless, discharging at 2C yields a very good agreement until approximately 12 As. Discrepancies appear at the end of the discharge process for 2C and 5C. Fig. 7f shows the results for the positive electrode. A very good agreement is also observed here for charging and discharging below C/2. In particular, charging at C/2 and discharging at 2C shows better agreement compared to the $D_s = const$ and *GITT-based* workflows. However, at the highest discharge rate of

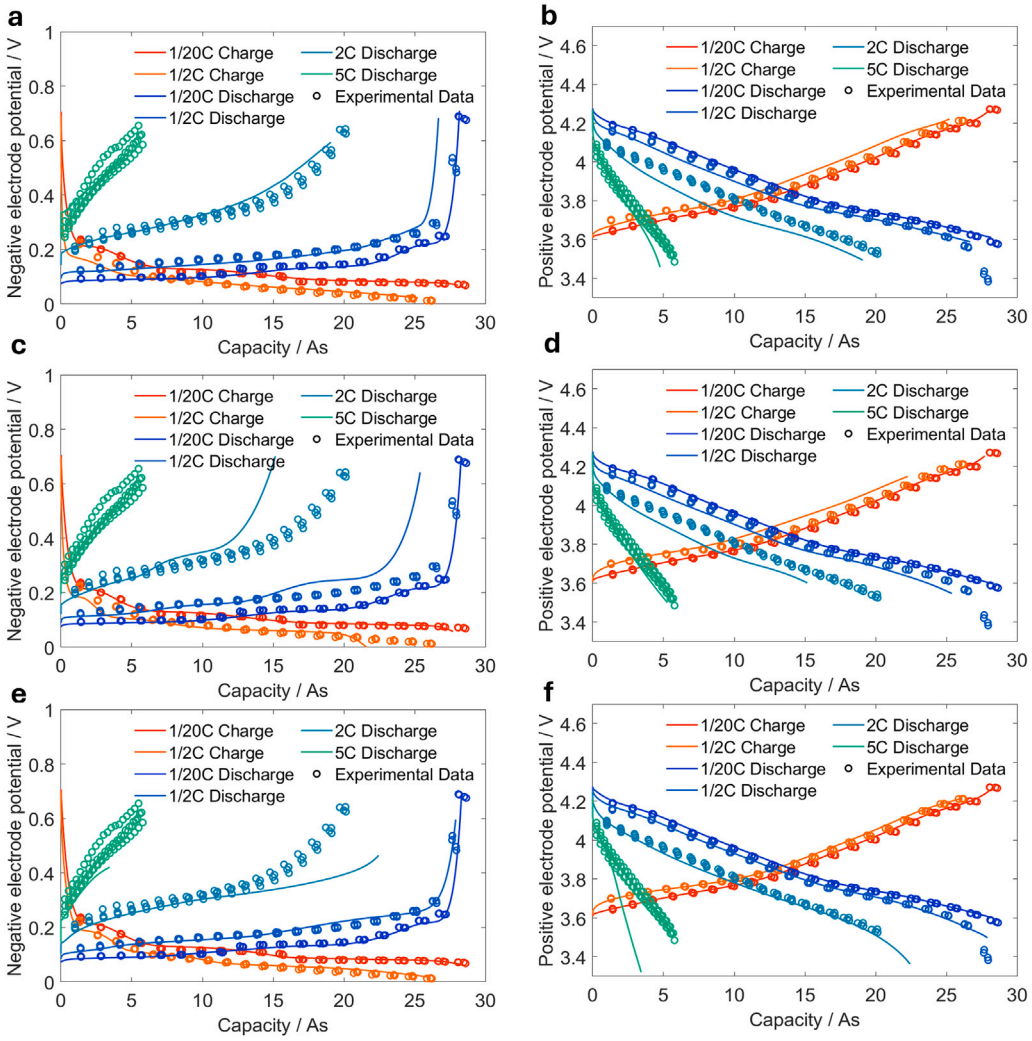

Fig. 7. Simulation results and experimental data for the C-rate test are plotted as electrode potential vs. capacity for (a) negative electrode for $D_s = const$ workflow, (b) positive electrode for $D_s = const$ workflow, (c) negative electrode for *GITT-based* workflow, (d) positive electrode for *GITT-based* workflow, (e) negative electrode for *PDF-based* workflow and (f) positive electrode for *PDF-based* workflow. Results are shown for C/20 and C/2 for charging and C/20, C/2, 2C and 5C for discharging. Simulation results are indicated as solid lines and experimental data points from four cells are indicated as circle markers for each plot.

5C, significant deviations are evident, which are higher than those of the other workflows.

In summary, good agreement is observed between the simulation and experiment for all workflows in C-rate tests. Overall, the fit for $D_s = const$ appears to be the closest to the experimental data. However, significant deviations are evident for discharging with 2C, in particular for the positive electrode. For C-rates smaller than C/2, the *PDF-based* workflow shows better agreement. This is especially surprising, given that the C-rate data was not used in this workflow. We believe that the deviations observed at higher C-rates in the *PDF-based* workflow could also be related to the model's inaccuracies, such as the assumption of uniform particle sizes and homogeneous electrodes. These inaccuracies might be compensated for in the other workflows by the parameter fitting procedure.

To validate the overall parameterization workflow and evaluate different approaches for determining diffusion coefficients, we analyzed the simulation error for WLTP driving cycles at various temperatures.

Fig. 8 presents the simulation and experimental results for the WLTP driving cycles at 25 °C for the three workflows. All simulations show excellent agreement with the experimental data, with respective RMSEs of 29.33 mV, 22.35 mV, and 15.88 mV for the $D_s = const$, *GITT-based*, and *PDF-based* workflows. Thus, the smallest RMSE at 25 °C is seen for the *PDF-based* workflow, though it has only a minimal advantage over the other workflows. It is important to note that the RMSE values represent the full cell voltage, meaning they include errors from both electrodes. The most noticeable deviations occur at 1700 s during a dynamic phase at lower SOC. Here, slight overestimation of the overpotential can be observed for the $D_s = const$ and *GITT-based* workflows. In contrast, the *PDF-based* workflow falls mostly within the range of the experimental data. However, the *PDF-based* workflow shows small deviations at approximately 500 s.

Further quantitative validation has been performed. The results are summarized in Table 1 This includes the RMSE of the Driving Cycle, Pulse Test, Capacity and Energy for Cycling with Variation of C-Rate at temperatures of 10 °C, 25 °C and 40 °C for all three workflows. Detailed results are shown in the SI.

For the WLTP Driving Cycle the error of $D_s = const$ is similar for all temperatures and ranges from 24.28 to 29.33 mV. In contrast, for the *GITT-based* workflow, the error significantly varies with temperature, being highest (44.26 mV) at the lowest temperature (10 °C) and lowest (15.55 mV) at the highest temperature (40 °C). The *PDF-based* workflow also shows similar errors for different temperatures, ranging from 15.88 to 29.95 mV. However, the deviations are more significant

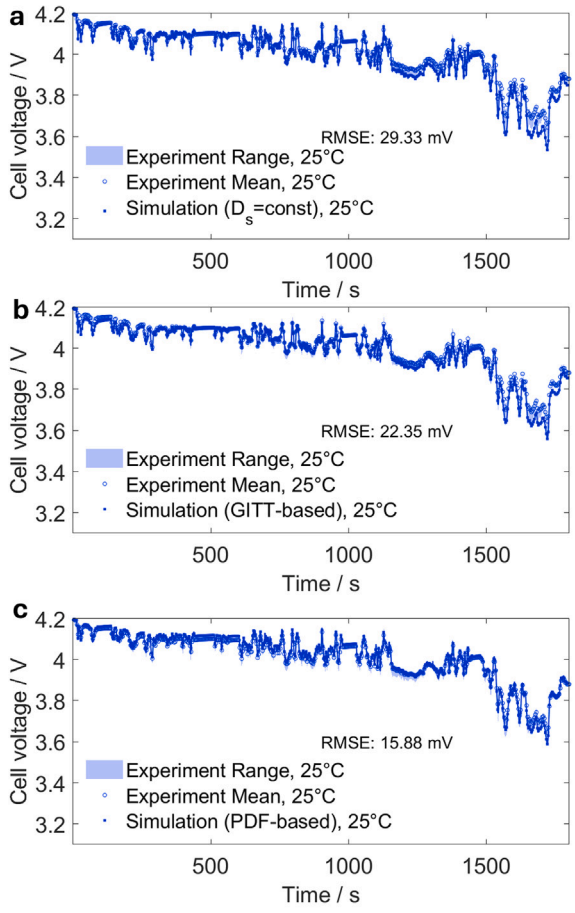

Fig. 8. Simulation and experimental data for WLTP driving cycles at 25 for (a) $D_s = const$, (b) *GITT-based* and (c) *PDF-based*. Filled circles show simulation results, empty circles shows mean of experimental results and colored area shows the range of the experimental results.

compared to the $D_s = const$ workflow. In particular, the error is higher at 10 °C.

The observed errors can be discussed further in consideration of the identified activation energies. The errors suggest that the temperature dependency of the diffusion coefficient, i.e., the activation energy of diffusion, is overestimated in the *GITT-based* workflow. This leads to high errors at low temperatures and low errors, likely compensating for other errors, at high temperatures. The activation energies for the *GITT-based* workflow are approximately 28 kJ mol^{-1} and 20 kJ mol^{-1} for the negative and positive electrodes, respectively. These values are significantly larger than the activation energies identified with the *PDF-based* workflow, which are approximately 8 kJ mol^{-1} and 10 kJ mol^{-1}, respectively. For the $D_s = const$ workflow, temperature dependency is neglected, leading to an activation energy of zero. Surprisingly, this workflow shows the most consistent error for different temperatures. However, it should be noted that, in general, overpotentials are expected to be lower at higher temperatures, so one might expect lower errors at higher temperatures.

Additionally, the RMSE for a profile with charge and discharge pulses at different SOCs has been evaluated. The results are also shown in Table 1. It can be seen that in general the lowest error is observed for the *PDF-based* workflow, which ranges from 7.61 mV to 18.63 mV. The error increases with decreasing temperature. This trend is also observed for the other workflows. However, they show in general higher errors. At 10 °C and 25 °C the highest error is observed for the *GITT-based* workflow. At 40 °C the highest error is observed for the $D_s = const$ workflow. In this additional test, again all workflows show good agreement with the experimental data. However, in contrast to the Driving Cycle the *PDF-based* workflow shows clearly the lowest error.

Further, in Table 1 the RMSE is shown for capacity and energy prediction for cycling with variation of the C-Rate. Detailed results are shown in the SI. For both values the same trend is seen. For 25 °C and 40 °C the *PDF-based* workflow shows the lowest error. At 10 °C, the lowest error is observed for the $D_s = const$ workflow, however with only minor advantage compared to the *PDF-based* workflow. For this validation the *GITT-based* workflow clearly shows the highest errors for all temperatures.

In conclusion, predicting full cell voltages shows that all three workflows are feasible options for parameterization when only full cell voltages are of interest. However, the *GITT-based* workflow shows increased errors, which is most distinct for cycling with variation of the C-Rate. Further, the results indicate that this workflow overestimates the activation energies. Nevertheless, between $D_s = const$ workflow and *PDF-based* workflow only minor differences have been observed until this point. The following section discusses the estimated parameters in detail to elaborate on the differences further.

Table 2 presents the results of the parameter estimation for tortuosity and electrical conductivity. For the $D_s = const$ and *GITT-based* workflow, these parameters are identified through parameter estimation using C-rate data. In contrast, for the *PDF-based* workflow, the parameters were identified using dedicated electrochemical experiments.

Significant differences can be seen. The highest tortuosity is observed for the $D_s = const$ workflow (16.63), and the lowest is observed for the *GITT-based* workflow (5.53). The *PDF-based* workflow lies in between (7.32). Usseglio-Viretta et al. provide a comprehensive study on tortuosity using various methods in Ref. [13]. Based on microstructure analysis, they determined the tortuosity of graphite in pores to range from 4.05 to 8.29. Both, the *GITT-based* workflow and the *PDF-based* workflow fall in this range. The tortuosity estimated by the $D_s = const$ workflow is significantly too large to be plausible. Note that the tortuosity determined by all workflows is directly related to porosity and the estimated electrode thickness from previous workflow steps. This could explain why the *PDF-based* workflow, which directly measures tortuosity, indicates values that are rather at the upper limit of the expected range. Furthermore, the electrodes characterized by Usseglio-Viretta et al. [13] are not the same electrodes, but only similar with respect to the active material. Strong calendaring of commercial electrodes might lead to higher tortuosity.

With respect to electrical conductivity of the negative electrode, both the $D_s = const$ and *GITT-based* workflows lead to values of approximately 0.1, which was set as the lower bound for parameter fitting. Graphite electrodes are expected to exhibit relatively high conductivity. Specifically, the literature reports negative electrode conductivities ranging from 6.6 to 250 S m^{-1} [9–11]. The directly measured conductivity of the *PDF-based* workflow is 0.58 S m^{-1}, which is higher than the other workflows but lower than expected.

For the tortuosity of the positive electrode significant deviations between the different workflows can be seen. The $D_s = const$ and *GITT-based* workflows lead to values of approximately 1, which was set as the lower bound for parameter fitting. However, the tortuosity measured directly in the *PDF-based* workflow is significantly higher (8.45). This value is also very high compared to those provided by Usseglio-Viretta et al. [13]. In that study, the tortuosity values for NMC cathodes ranged from 2 to 4. It should be noted that they did not characterize the same electrode, only similar materials. For the commercial electrodes characterized here, indications of heavy calendaring have been observed, i.e., cracking of particles and deformation of the aluminum foil. This is also visible in the microscopy pictures shown in the SI. Therefore, high tortuosity is expected, though, considering

Usseglio-Viretta et al. [13], the measured tortuosity still seems high for a NMC electrode. Nevertheless, the very low values estimated by $D_s = const$ and *GITT-based* methods are not plausible, as they indicate direct ionic pathways, i.e., no tortuosity.

Significant deviations are also visible for the positive electrode in the conductivity results. The highest values are seen in the *GITT-based* workflow (84.18 S m^{-1}), followed by the $D_s = const$ workflow (17.25 S m^{-1}). Direct measurements in the *PDF-based* workflow show orders of magnitude lower values (0.25 S m^{-1}), which are slightly lower than the conductivity measured for the negative electrode.

The observed differences in estimated tortuosity and electrical conductivity are discussed further in light of the previously shown diffusion coefficients (Fig. 5). For the negative electrode, the identified constant diffusion coefficient ($D_s = const$ workflow) is generally higher than the diffusion coefficient in the *GITT-based* and *PDF-based* workflows. This explains why the identified tortuosity is much higher; it can compensate for an overestimation of solid-state diffusion by limiting electrolyte diffusion. Similarly, the *GITT-based* diffusion coefficients are generally lower than the *PDF-based* values. This can be compensated for by lowering the tortuosity.

The observed differences in tortuosity are even more significant for the positive electrode. The identified constant diffusion coefficient for the $D_s = const$ workflow is mostly higher compared to the *GITT-based* workflow, but lower than for the *PDF-based* workflow. This explains why tortuosity is estimated to be higher compared to the *GITT-based* workflow. However, the most notable observation is that tortuosity for both the $D_s = const$ and *GITT-based* workflows is significantly lower compared to the *PDF-based* workflow. This can be explained, because the diffusion coefficient of the *PDF-based* workflow is generally higher, and therefore the tortuosity the other workflows must be lower. Further, the high diffusion coefficient is also compensated by the low electrical conductivity, which is orders of magnitude lower than that of the other workflows. Remarkably, despite these significant differences in parameters for the positive electrode, only minor differences are observed in C-rate tests and dynamic driving cycles.

4. Conclusions

In this study, we used three heuristic workflows to perform P2D model parameterization. These workflows included direct measurements at the electrode level and parameter estimation. Our goal was to identify reliable, physically meaningful parameters for commercial LIBs. We demonstrated that different methods of determining the diffusion coefficient can lead to significant discrepancies in parameter sets.

The diffusion coefficient can be determined using GITT analysis. However, the assumptions underlying GITT do not allow application in two-phase regions and disregard other contributions to pulse polarization, such as diffusion processes in the electrolyte. Flat OCPs in two-phase regions usually result in very small diffusion coefficients. Therefore, measurements that do not satisfy the GITT assumptions must be excluded. In general, all points measured within flat regions must be disregarded. We propose a method to estimate the error associated with GITT measurements. Based on this error estimation, valid GITT measurement points can be selected. One remaining challenge is the limited availability of valid datapoints in material like graphite, as only few have low relative errors. In particular, no valid values were available at DOLs greater than 0.5. We further analyzed the influence of electrolyte processes on pulse polarization and GITT analysis using the P2D model. It was shown that error significantly depends on the gradient of the OCP. However, even with steep gradients, the error exceeded 20%, leading to a significant underestimation of the diffusion coefficient. With more and more flat OCPs, the error quickly increases. Theoretically, pulse polarization does not show any sensitivity to the diffusion coefficient for zero gradients. Therefore, it is necessary to take electrolyte diffusion into account while evaluating GITT data.

The uncertainty of the diffusion coefficient was further analyzed by determining the PDF of the diffusion coefficient for the positive and negative electrodes. Considering directly measured tortuosity and electrical conductivity, the highest probabilities of the diffusion coefficient were found at significantly higher values compared to the GITT analysis. This was particularly the case for the positive electrode. This method has been integrated in a parameterization workflow, referred to as *PDF-based*.

We investigated the validity of three possible workflows, $D_s = const$, *GITT-based*, *PDF-based*, that handle diffusion coefficient identification differently. To this end, we evaluated the results for electrode potentials in C-rate test simulation. We further conducted a extended validation experiment that includes pulse tests, cycling with variation of the C-Rate and dynamic WLTP cycles and used it to provide a quantitative validation of the parameterization workflows. We also discussed the differences in the identified parameter sets, e.g., diffusion coefficients, tortuosity, and electrical conductivity. Overall, we demonstrated that all three workflows lead to good agreement in both C-rate tests and dynamic WLTP cycles. The $Ds = const$ workflow showed the best agreement with the C-rate tests. However, at C-rates smaller than C/2, the *PDF-based* workflow's agreement was superior. This is remarkable because, unlike the other workflows, the C-rate test data was not used for parameter fitting. Furthermore, during charging at 0.5 C, the *GITT-based* workflow results in a significantly earlier decline of the negative electrode potential, which is associated with an overestimation of lithium plating offset. This aspect is better covered by the $Ds = const$ and *GITT-based* workflows. All workflows lead to good agreement in dynamic driving cycles. However, for validation using cycling experiments with variation of the C-Rate, the *GITT-based* workflow showed significantly higher errors. Further, the results indicate that, for the *GITT-based* workflow, temperature dependency, i.e., activation energies, is overestimated, which leads to larger errors at low temperatures. The most distinct differences are observed with respect to the estimated parameters. For the negative electrode, $Ds = const$ seems to overestimate tortuosity, while for the positive electrode, $Ds = const$ and *GITT-based* workflows underestimate tortuosity. *PDF-based* workflows measure tortuosity directly and lead to plausible, albeit rather high, tortuosity values. However, it is noted that these values are also related to the assumed electrolyte parameters and the electrode thickness and porosity estimated in earlier steps. Finally, for commercial electrodes, high calendaring degrees and, consequently, high tortuosity are expected. Additionally, it is observed that the differences between the workflows depend on the electrode. For example, for the positive electrode, the $Ds = const$ workflow leads to tortuosity values much smaller than the directly measured values, while for the negative electrode, the values are significantly larger.

Our results indicate that the *PDF-based* workflow allows to overcome the limitation of classical *GITT-based* workflows, which enables an overall plausible parameter set and good agreement with experimental data for C-rate tests, pulse tests at different SOCs, cycling with variation of C-Rate and dynamic WLTP cycles. The drawback is that electrical conductivity and tortuously need to be measured with additional experiments. Nevertheless, the workflow only requires classical electrochemical and optical characterization on electrode level making it feasible for the parameterization of P2D models of commercial battery electrodes.

In summary, the presented work elaborates on the uncertainties related to the parameterization of the P2D model for commercial battery electrodes and the determination of the solid-state diffusion coefficient. We employ this method for a *PDF-based* parameterization and compare its validity to two common workflows used for PD2 model parameterization, which shows good agreement to experimental data and a plausible parameter set.

In this work, the workflows has been applied for a battery cell based on state of the art materials. However, currently it is not clear to what extend the workflow can be transferred for other material classes. As

shown in this work, particularly for materials with flat OCPs, such as LFP, the application of CC pulses to determine the diffusion coefficient is a remaining challenge [21,26]. Further, materials with strong hysteresis of the OCP or other parameters, i.e. materials with significant short term path dependency, need to addressed in future [33]. Also for blend materials or significant deviations in particle sizes the presented methods need to be extended, as here each particle contributes to the current pulse response [34]. In all cases outlined, the presented methodology can serve as a baseline. In this work, the battery cell has been parameterized at the BOL. However, the parameters can evolve over the cell's lifetime due to aging. Previous studies have shown that aging related parameters can be updates using suitable characterization or check-up cycles [35,36], which preserves the predictive capability of physics-based models and provides insight into the underlying physical aging processes. In this context, EIS is particularly promising, as it allows individual process contributions to cell-to-cell variability to be identified [37,38]. Degradation pathways can be further analyzed through degradation mode analysis [39,40]. This enables to update model parameter, e.g. loss of active material at the positive electrode can be represented by a reduced active material fraction in the P2D model. A major limitation for the parameter adjustment in practical application is data scarcity, as idealized characterization cycles are often not available. This issue is especially critical for second-use applications, where battery histories are incomplete [41]. In addition, second-use datasets are heterogeneous, with insufficient information on cell chemistry [42]. Nevertheless, if second-use data can be leveraged to infer parameter changes or to select previously identified parameter sets, physics-based models can become efficient tools for sorting retired batteries. However, outcome will be highly sensitive to the initial model parameters, which can significantly vary depending on parameterization workflow as shown in this work. Future work may investigate the application of generative learning methods as proposed by Tao et al. [41] in combination with models at BOL to rapidly estimate parameter variations, enabling cell grouping strategies that extend beyond capacity-based sorting.

Future work should also extend the validation to larger scales, e.g. pouch cell, module and system level to investigate the applicability to real operating conditions, which will also support the application of a parameterized model in the field. In addition, investigation of the reliability of these parameterization workflows in aging diagnosis and second-use classification should be addressed. Finally, combining the proposed workflows with advanced experimental design and data-driven methods can further reduce experimental time and effort needed for model parameterization.

CRediT authorship contribution statement

F. Röder: Writing – review & editing, Writing – original draft, Visualization, Validation, Supervision, Software, Resources, Project administration, Methodology, Investigation, Funding acquisition, Formal analysis, Data curation, Conceptualization. **H. Harimi:** Validation, Methodology, Investigation, Data curation. **F. Schomburg:** Methodology, Investigation, Formal analysis, Data curation, Conceptualization. **M. Han:** Methodology, Investigation, Formal analysis, Data curation. **J.C. Wurzenberger:** Writing – review & editing, Supervision, Resources, Investigation, Funding acquisition, Conceptualization. **C. Lechner:** Writing – review & editing, Methodology, Investigation. **S. Kutschi:** Writing – review & editing, Supervision, Project administration, Investigation, Conceptualization.

Declaration of Generative AI and AI-assisted technologies in the writing process

During the preparation of this work the authors used ChatGPT and DeepL Write in order to improve the readability and to perform spell checking. After using these tools, the authors reviewed and edited the content as needed and take full responsibility for the content of the published article.

Declaration of competing interest

The authors declare that they have no known competing financial interests or personal relationships that could have appeared to influence the work reported in this paper.

Acknowledgments

The authors would like to express their sincere gratitude to the European Union for supporting this work under the project 101103628 AccCellBaT. This work was also partially supported by the project "ILAB" (03XP0467) by the Federal Ministry of Education and Research in Germany (BMBF). Further, support by the BayBatt Cell Technology Center is gratefully acknowledged, funded by the Deutsche Forschungsgemeinschaft (DFG, German Research Foundation), Germany—INST 91/452-1 LAGG. We further thank Berk Oguz for his support in preparing cells for electrochemical characterization and Philipp Rank and Daniel Leykam for discussing mechanical and electrical characterization and conducting the mechanical characterization of the separator.

Appendix A. Supplementary data

Supplementary material related to this article can be found online at https://doi.org/10.1016/j.jpowsour.2026.239594.

Data availability

Data will be made available on request.

References

[1] M. Doyle, T. Fuller, J. Newman, Modeling of galvanostatic charge and discharge of the lithium/polymer/insertion cell, J. Electrochem. Soc. 140 (1993) 1526.
[2] F. Röder, S. Sonntag, D. Schröder, U. Krewer, Simulating the impact of particle size distribution on the performance of graphite electrodes in lithium-ion batteries, Energy Technol. 4 (2016) 1588–1597.
[3] O. Schmidt, F. Röder, Conductive networks and their impact on uncertainty, degradation, and failure of lithium-ion battery electrodes, ACS Appl. Energy Mater. 4 (2021) 4845–4860.
[4] J. Foster, Y. Grudeva, I. Korotkin, E. Dickinson, G. Offer, G. Richardson, The Newman model for phase-change electrodes: Physics-based hysteresis, J. Electrochem. Soc. 172 (2025).
[5] S. O'Kane, W. Ai, G. Madabattula, D. Alonso-Alvarez, R. Timms, V. Sulzer, J. Edge, B. Wu, G. Offer, M. Marinescu, Lithium-ion battery degradation: How to model it, Phys. Chem. Chem. Phys. 24 (2022) 7909–7922.
[6] F. Bahiraei, M. Ghalkhani, A. Fartaj, G. Nazri, A pseudo 3D electrochemical-thermal modeling and analysis of a lithium-ion battery for electric vehicle thermal management applications, Appl. Therm. Eng. 125 (2017) 904–918.
[7] M. Andersson, M. Streb, J. Ko, V. Löfqvist Klass, M. Klett, H. Ekström, M. Johansson, G. Lindbergh, Parametrization of physics-based battery models from input–output data: A review of methodology and current research, J. Power Sources 521 (2022) 230859.
[8] K. Liu, Y. Gao, C. Zhu, K. Li, M. Fei, C. Peng, X. Zhang, Q. Han, Electrochemical modeling and parameterization towards control-oriented management of lithium-ion batteries, Control Eng. Pract. 124 (2022) 105176.
[9] C. Chen, F. Planella, K. O'Regan, D. Gastol, W. Widanage, E. Kendrick, Development of experimental techniques for parameterization of multi-scale lithium-ion battery models, J. Electrochem. Soc. 167 (2020) 080534.
[10] M. Ecker, T. Tran, P. Dechent, S. Käbitz, A. Warnecke, D. Sauer, Parameterization of a physico-chemical model of a lithium-ion battery: I. determination of parameters, J. Electrochem. Soc. 162 (2015) A1836.
[11] L. Oca, E. Miguel, E. Agirrezabala, A. Herran, E. Gucciardi, L. Otaegui, E. Bekaert, A. Villaverde, U. Iraola, Physico-chemical parameter measurement and model response evaluation for a pseudo-two-dimensional model of a commercial lithium-ion battery, Electrochim. Acta 382 (2021) 138287.
[12] J. Schmalstieg, C. Rahe, M. Ecker, D. Sauer, Full cell parameterization of a high-power lithium-ion battery for a physico-chemical model: Part I. physical and electrochemical parameters, J. Electrochem. Soc. 165 (2018) A3799.
[13] F. Usseglio-Viretta, A. Colclasure, A. Mistry, K. Claver, F. Pouraghajan, D. Finegan, T. Heenan, D. Abraham, P. Mukherjee, D. Wheeler, et al., Resolving the discrepancy in tortuosity factor estimation for Li-Ion battery electrodes through micro-macro modeling and experiment, J. Electrochem. Soc. 165 (2018) A3403–A3426.

[14] E. Miguel, G. Plett, M. Trimboli, L. Oca, U. Iraola, E. Bekaert, Review of computational parameter estimation methods for electrochemical models, J. Energy Storage 44 (2021) 103388.
[15] L. Xu, X. Lin, Y. Xie, X. Hu, Enabling high-fidelity electrochemical P2D modeling of lithium-ion batteries via fast and non-destructive parameter identification, Energy Storage Mater. 45 (2022) 952–968.
[16] Z. Khalik, M. Donkers, J. Sturm, H. Bergveld, Parameter estimation of the Doyle–Fuller–Newman model for lithium-ion batteries by parameter normalization, grouping, and sensitivity analysis, J. Power Sources 499 (2021) 229901.
[17] V. Laue, F. Röder, U. Krewer, Practical identifiability of electrochemical P2D models for lithium-ion batteries, J. Appl. Electrochem. 51 (2021) 1572–8838.
[18] C. Zhang, Y. Guo, C. Wang, S. Li, O. Curnick, T. Amietszajew, R. Bhagat, A new design of experiment method for model parametrisation of lithium ion battery, J. Energy Storage 50 (2022) 104301.
[19] J. Günther, D. Wycisk, R. Siva Dev, A. Fill, K. Birke, R. Moos, J. Philipp Schmidt, M. Oldenburger, Determination of the solid state diffusion coefficient of Li-Ion battery single-phase materials using thin model electrodes, J. Electrochem. Soc. 172 (2025) 030525.
[20] M. Cabañero, N. Boaretto, M. Röder, J. Müller, J. Kallo, A. Latz, Direct determination of diffusion coefficients in commercial Li-Ion batteries, J. Electrochem. Soc. 165 (2018) A847.
[21] Y. Zhu, T. Gao, X. Fan, F. Han, C. Wang, Electrochemical techniques for intercalation electrode materials in rechargeable batteries, Acc. Chem. Res. 50 (2017) 1022–1031.
[22] M. Ball, M. Cormier, E. Zsoldos, I. Haman, S. Yu, N. Zhang, N. Phattharasupakun, M. Johnson, M. Metzger, C. Yang, J. Dahn, Method—AMIDR: A complete pulse method for measuring cathode solid-state diffusivity, J. Electrochem. Soc. 171 (2024) 020552.
[23] J. Horner, G. Whang, D. Ashby, I. Kolesnichenko, T. Lambert, B. Dunn, A. Talin, S. Roberts, Electrochemical modeling of GITT measurements for improved solid-state diffusion coefficient evaluation, ACS Appl. Energy Mater. 4 (2021) 11460–11469.
[24] S. Kang, W. Chueh, Galvanostatic intermittent titration technique reinvented: Part I. a critical review, A Crit. Rev. J. Electrochem. Soc. 168 (2021) 120504.
[25] A. Nickol, T. Schied, C. Heubner, M. Schneider, A. Michaelis, M. Bobeth, G. Cuniberti, GITT analysis of lithium insertion cathodes for determining the lithium diffusion coefficient at low temperature: Challenges and pitfalls, J. Electrochem. Soc. 167 (2020) 090546.
[26] Y. Zhu, C. Wang, Galvanostatic intermittent titration technique for phase-transformation electrodes, J. Phys. Chem. C 114 (2010) 2830–2841.
[27] X. Yang, A. Rogach, Electrochemical techniques in battery research: A tutorial for nonelectrochemists, Adv. Energy Mater. 9 (2019) 1900747.
[28] C. Schmitt, M. Gerle, D. Kopljar, K. Friedrich, Full parameterization study of a high-energy and high-power Li-Ion cell for physicochemical models, J. Electrochem. Soc. 170 (2023) 070509.
[29] J. Landesfeind, J. Hattendorff, A. Ehrl, W. Wall, H. Gasteiger, Tortuosity determination of battery electrodes and separators by impedance spectroscopy, J. Electrochem. Soc. 163 (2016) A1373.
[30] A. Colclasure, R. Kee, Thermodynamically consistent modeling of elementary electrochemistry in lithium-ion batteries, Electrochim. Acta 55 (2010) 8960–8973.
[31] J. Landesfeind, H. Gasteiger, Temperature and concentration dependence of the ionic transport properties of lithium-ion battery electrolytes, J. Electrochem. Soc. 166 (2019) A3079.
[32] N. Legrand, S. Raël, B. Knosp, M. Hinaje, P. Desprez, F. Lapicque, Including double-layer capacitance in lithium-ion battery mathematical models, J. Power Sources 251 (2014) 370–378.
[33] F. Röder, S. Ramasubramanian, A review and perspective on path dependency in batteries, Energy Technol. 10 (2022) 2200627.
[34] T. Liebmann, C. Heubner, M. Schneider, A. Michaelis, Understanding kinetic and thermodynamic properties of blended cathode materials for lithium-ion batteries, Mater. Today Energy 22 (2021) 100845.
[35] D. Witt, F. Röder, U. Krewer, Analysis of lithium-ion battery state and degradation via physicochemical cell and SEI modeling, Batteries & Supercaps 5 (2022) e202200067.
[36] G. Sordi, A. Stecchini, R. Evangelista, D. Luder, W. Li, D. Sauer, A. Casalegno, C. Rabissi, Degradation of lithium-ion batteries under automotive-like conditions: P2D model-based understanding and ex-situ validation, ETransportation 24 (2025) 100410.
[37] T. Rüther, M. Schamel, C. Plank, F. Schomburg, F. Röder, M. Danzer, Cell-to-cell variation beyond parameter analysis — Identification and correlation of processes in lithium-ion batteries using a combined distribution of relaxation times analysis, J. Power Sources 587 (2023) 233677.
[38] T. Rüther, C. Plank, M. Schamel, M. Danzer, Detection of inhomogeneities in serially connected lithium-ion batteries, Appl. Energy 332 (2023) 120514.
[39] R. Li, N. Kirkaldy, F. Oehler, M. Marinescu, G. Offer, S. O'Kane, The importance of degradation mode analysis in parameterising lifetime prediction models of lithium-ion battery degradation, Nat. Commun. 16 (2025) 2776.
[40] S. Ramasubramanian, C. Plank, M. Danzer, F. Röder, Degradation path indicators for lithium-ion batteries, J. Energy Storage 140 (2025) 119113.
[41] S. Tao, R. Ma, Z. Zhao, G. Ma, L. Su, H. Chang, Y. Chen, H. Liu, Z. Liang, T. Cao, et al., Generative learning assisted state-of-health estimation for sustainable battery recycling with random retirement conditions, Nat. Commun. 15 (2024) 10154.
[42] S. Tao, H. Liu, C. Sun, H. Ji, G. Ji, Z. Han, R. Gao, J. Ma, R. Ma, Y. Chen, et al., Collaborative and privacy-preserving retired battery sorting for profitable direct recycling via federated machine learning, Nat. Commun. 14 (2023) 8032.